PHILOSOPHICAL TRANSACTIONS OF THE ROYAL SOCIETY A MATHEMATICAL, PHYSICAL & ENGINEERING SCIENCES

Radially symmetric ice sheet flow

L. W. Morland

Phil. Trans. R. Soc. Lond. A 1997 **355**, 1873-1904
doi: 10.1098/rsta.1997.0094

Radially symmetric ice sheet flow

By L. W. Morland

School of Mathematics, University of East Anglia, Norwich NR4 7TJ, UK

The evolution equations for a radially symmetric grounded ice sheet flowing under gravity are formulated on the basis that the ice is an incompressible nonlinearly viscous heat conducting fluid with temperature-dependent rate factor. The reduced model, which comprises the leading order balances when longitudinal gradients are small compared with gradients through the sheet thickness, is derived. Steady flow is analysed when the temperature field is prescribed, uncoupled from the energy balance or satisfying energy balance with the addition of an appropriate heat source. The problem reduces to a second-order differential equation for the thickness with boundary conditions at the divide (axis of symmetry) and margin, with the margin radius unknown. Asymptotic analysis yields an expression for the surface slope at the margin. Numerical algorithms for both non-slip and sliding at the base are constructed and tested against solutions of special cases. A variety of examples are solved to demonstrate the influence of the viscous law, surface accumulation distribution, sliding and the bed form for different prescribed temperature fields; including evaluation of the heat source distribution necessary to maintain the temperature field.

1. Introduction

Realistic simulations of ice sheet evolution hinge on large scale numerical computation. A sound physical description of the ice response to stress and temperature, and of the interactions with the atmosphere and bed, are essential features, but the model equations based on any set of sensible physical assumptions define a complex initial/boundary-value problem on the unknown ice sheet domain. It is recognized that while the polycrystalline aggregates of newly formed ice in the surface of an ice sheet contain random distributions of crystal axes, and so respond isotropically on length scales of interest, an ice fabric with preferred direction(s) develops as the ice descends to depth, giving rise to induced anisotropic response. A recent European Ice Sheet Modelling Initiative (EISMINT) Workshop (Aussois, January 1994) debated the current understanding of fabric evolution and focused attention on the theoretical developments necessary to construct an anisotropic constitutive model consistent with observations of fabric in deep core samples. At present there is no established anisotropic law to underpin ice sheet modelling, and current theory and computation are based on the long-standing assumption of an incompressible nonlinearly viscous fluid (necessarily isotropic) with strongly temperature dependent rate factor. A detailed account of this theory, both its background and mathematical developments, are presented in Hutter (1983), and Morland's (1993) lectures.

In view of the scale and complexity of computations of the full isotropic model

Phil. Trans. R. Soc. Lond. A (1997) **355**, 1873–1904
Printed in Great Britain

equations for a grounded ice sheet, which have not yet been performed, current applications are based on a simplified *reduced model* which exploits the large aspect ratio of natural ice masses, described by Hutter (1983) as the 'shallow ice approximation'. The reduced model equations are the leading order balances derived from asymptotic series expansions in a small parameter ε which can be viewed as a measure of the thickness to span ratio, or the corresponding ratio of velocity components, but more precisely it is a small parameter reflecting the ratio of gradients in longitudinal directions to those in the thickness direction, which is determined explicitly by the balances. Systematic approximations of equations describing a variety of glaciology applications by asymptotic series and coordinate stretching were first developed by Fowler (1977, 1979*a*,*b*), Fowler & Larson (1978), Morland & Johnson (1980, 1982), Hutter (1981, 1982*a*,*b*, 1983), Hutter *et al.* (1982), Morland (1982) and Morland & Smith (1984), and specifically for floating ice shelves by Morland & Shoemaker (1982), Morland (1985) and Morland & Zainuddin (1985). Morland & Johnson (1980, 1982) identified and derived explicitly the distinct small coordinate stretching parameter ε for ice sheets on horizontal or near horizontal mean bed planes, and for glaciers on steep beds that are nearly plane, in the restricted case of steady isothermal plane flow, extended to steady plane flow with a prescribed temperature field by Morland & Smith (1984), and the general unsteady three-dimensional formulation was presented by Hutter (1983) and Morland (1984). It must be emphasized that the validity of the leading order balances fails whenever a longitudinal gradient is not of order ε compared to a thickness gradient, and hence fails whenever the bed form slope is finite.

A significant feature of the reduced model equations is that they can be formally integrated through the thickness in both steady and unsteady cases to eliminate one spatial coordinate when the temperature field is prescribed (Morland & Smith 1984), without the invalid approximations of earlier depth integrated flow line models (Morland 1993). The simpler isothermal steady plane flow situation (Morland & Johnson 1980, 1982) allowed explicit integrations and algebraic construction of the ordinary differential equation governing the surface elevation. Furthermore, the essential nonlinearity of the second-order differential equation arising for the small mean bed plane slope allowed the determination of a unique bounded surface slope at a margin given a particular form of sliding law there, which converted the two-point boundary-value problem to a simpler initial value problem. This also followed for the steady plane flow with a prescribed temperature field. In the radially symmetric steady flow application described herein, a margin analysis again determines the unique bounded surface slope with the chosen sliding law, and the asymptotic form of the unbounded slope in the case of non-slip, but there is still a boundary-value problem with conditions at both margin and divide. It will be demonstrated that conversion to an initial value problem in the plane flow case is strictly a special situation.

Prescribing a temperature field ignores the energy balance. However, a prescription can qualitatively echo observed temperature profiles, and satisfy required surface and base thermal boundary conditions, and so provides a sensible basis for investigating the effects of varying temperature through the ice sheet with consequent strongly varying rate factor in the viscous response, in contrast to isothermal approximations. Provided that the prescribed temperature field is twice continuously differentiable, it is the solution of a coupled energy balance with an added smooth heat source distribution which is determined by the prescribed temperature solution. This solu-

tion is then that of thermomechanically coupled reduced equations with the same boundary conditions and an additional algebraic heat source distribution which does not change the differential structure of the equations. It therefore provides a comparison solution for a direct computation of the coupled equations, and in the case of steady two-dimensional flow, plane or radially symmetric, this solution is determined by routine numerical integration of a system of ordinary differential equations and, furthermore, can be verified by an integral property of the original equations. That is, algorithms for direct computation of the coupled, reduced or full equations can be assessed, at least to the accuracy with which they can solve small bed slope problems in a simple geometry, which is a necessary, though not sufficient, condition for their validity. It is reasonable to assert that if an evolution algorithm determines a correct long time limit steady solution, and if the evolution equations reflect a unique physical response of the ice sheet, then its performance during the evolution is sound. There is possible non-uniqueness of the limit solution, which may yield distinct spans and profiles for different initial conditions, but a predicted solution can be verified to be, or not, consistent with the corresponding prescribed temperature solution.

EISMINT Workshops on Model Intercomparisons (Brussels, June 1993; Bremerhaven, June 1994), Huybrechts & Payne (1996), proposed and compared solutions obtained numerically for simple test problems by different modelling groups. The algorithms were all based on the reduced model, or a more restricted model. Good agreement for the profile prediction was obtained, but not for the temperature field. Since temperature has a strong influence on the viscous response of the ice, there is clearly an uncertainty in some, if not all, the algorithms, but in any case, agreement between similar numerical approaches does not guarantee that a correct solution has been reached. The construction of highly accurate, verified, comparison solutions offers an important necessary validation criteria for the large-scale algorithms which are necessary to treat more realistic problems.

The full equations for radially symmetric flow of a grounded ice sheet are presented below, together with the corresponding reduced model. Formal depth integration is carried out for a prescribed temperature field and the second-order ordinary differential equation for the thickness is derived in the steady flow case. Analysis of the margin fields determines a unique surface slope at the margin for the chosen form of sliding law and for the asymptotic form of the unbounded slope in the case of non-slip at the bed. Analysis of the divide behaviour shows that all terms in the differential equation are bounded there. This theory is an application of the general three-dimensional theory developed in Morland (1984). A direct numerical treatment of the coupled reduced model, with temperature governed by an energy balance incorporating heat advection, was carried out for a steady axisymmetric ice sheet by Hutter *et al.* (1987). They made comparisons with plane flow and investigated the influence of thermal boundary conditions, surface accumulation and basal sliding. The present analytic progress is possible only for the uncoupled, prescribed temperature theory.

Next, different coordinate transformations are introduced for the non-slip and sliding cases to construct a system of three ordinary differential equations on a fixed range, with all derivatives bounded, which form a two-point boundary-value problem to determine the span (margin radius) and thickness profile. Numerical algorithms for their solutions are presented and verified by test problems. Moreover, an integral property of the original reduced model equations allows the accuracy at each integration step to be verified. Examples are solved to illustrate the effects of a pre-

scribed temperature distribution compared with an isothermal approximation, of the prescribed surface accumulation, of a prescribed bed form compared with a flat bed and of the non-slip basal condition compared with sliding with different friction parameters. These selected examples provide a range of tests for the accuracy of direct algorithms when such features are varied.

2. Radially symmetric flow

The ice sheet profile and all associated physical variables are supposed to be radially symmetric about an axis $0z$ ($r = 0$), depending only on (r, z) in cylindrical polar coordinates (r, θ, z) with $0z$ vertically upwards. Since the flow is gravity driven, this symmetry implies that the mean bed plane is horizontal, say $z = 0$. A rigid bed form $z = f(r)$ is prescribed in the present analysis, eliminating consideration of the motion of deformable bed and its matching with that of the ice across an unknown basal interface. The ice sheet surface is defined by $z = h(r, t)$, where t denotes time and h is part of the flow solution to be determined. The physical components of the velocity, strain-rate and stress are, respectively,

$$\boldsymbol{v} = (v_r, 0, v_z), \tag{2.1}$$

$$\boldsymbol{D} = \begin{pmatrix} \dfrac{\partial v_r}{\partial r} & 0 & \dfrac{1}{2}\left[\dfrac{\partial v_r}{\partial z} + \dfrac{\partial v_z}{\partial r}\right] \\ 0 & \dfrac{v_r}{r} & 0 \\ \dfrac{1}{2}\left[\dfrac{\partial v_r}{\partial z} + \dfrac{\partial v_z}{\partial r}\right] & 0 & \dfrac{\partial v_z}{\partial z} \end{pmatrix}, \tag{2.2}$$

$$\boldsymbol{\sigma} = \begin{pmatrix} \sigma_{rr} & 0 & \sigma_{rz} \\ 0 & \sigma_{\theta\theta} & 0 \\ \sigma_{rz} & 0 & \sigma_{zz} \end{pmatrix}. \tag{2.3}$$

It is supposed that stress is measured relative to a uniform atmospheric isotropic pressure.

Mass conservation and incompressibility are satisfied by

$$\frac{\partial v_r}{\partial r} + \frac{v_r}{r} + \frac{\partial v_z}{\partial z} = 0, \tag{2.4}$$

and the ice density is assumed to be uniform with value $\rho = 918\,\mathrm{kg\,m^{-3}}$. The very slow flow of ice sheets yields particle accelerations that are extremely small compared to gravity and stress gradient contributions to the momentum balances, which become the equilibrium equations

$$\frac{\partial \sigma_{rr}}{\partial r} + \frac{\sigma_{rr} - \sigma_{\theta\theta}}{r} + \frac{\partial \sigma_{rz}}{\partial z} = 0, \tag{2.5}$$

$$\frac{\partial \sigma_{rz}}{\partial r} + \frac{\sigma_{rz}}{r} + \frac{\partial \sigma_{zz}}{\partial z} - \rho g = 0, \tag{2.6}$$

where g is the constant acceleration due to gravity, $9.81\,\mathrm{m\,s^{-2}}$. The θ equilibrium is automatically satisfied because of the symmetry assumption. The ice is assumed to have internal energy depending only on temperature T, with constant specific heat $C = 2 \times 10^3\,\mathrm{N\,m\,kg^{-1}\,K^{-1}}$, and satisfy a linear heat conduction law with constant

thermal conductivity $\lambda = 2.2\ \mathrm{N\ K^{-1}\ s^{-1}}$. Assuming cold ice throughout the interior, that is, no internal melting (phase change), energy conservation requires

$$\frac{\partial T}{\partial t} + v_r \frac{\partial T}{\partial r} + v_z \frac{\partial T}{\partial z} = \frac{\lambda}{\rho C}\left(\frac{\partial^2 T}{\partial r^2} + \frac{1}{r}\frac{\partial T}{\partial r} + \frac{\partial^2 T}{\partial z^2}\right) + \frac{1}{\rho C}\,\mathrm{tr}(\boldsymbol{\sigma D}) + \frac{s}{\rho C}, \tag{2.7}$$

where s is the heat source per unit volume; for example, radiation penetration near the surface. The stress-working contribution may be significant in basal regions.

In terms of the deviatoric stress

$$\hat{\boldsymbol{\sigma}} = \boldsymbol{\sigma} + p\mathbf{1}, \quad p = -\tfrac{1}{3}\,\mathrm{tr}\,\boldsymbol{\sigma}, \tag{2.8}$$

where p is the mean pressure, the nonlinearly viscous shear response of the ice is assumed to have the form

$$\frac{\boldsymbol{D}}{D_0} = a(T)\psi(J)\frac{\boldsymbol{\sigma}}{\sigma_0}, \tag{2.9}$$

where

$$J = \tfrac{1}{2}\,\mathrm{tr}\left(\frac{\boldsymbol{\sigma}}{\sigma_0}\right)^2, \tag{2.10}$$

which is the commonly adopted viscous simplification with $\hat{\boldsymbol{\sigma}}$ parallel to $\boldsymbol{D}$ and the response coefficient ψ depending only on one invariant J of $\hat{\boldsymbol{\sigma}}$, and with a multiplying temperature dependent rate factor $a(T)$. The units σ_0 and D_0 are chosen to normalize the coefficient ψ over a shear stress range 0–$10^5\ \mathrm{N\ m^{-2}}$ at near-melting temperature, but the significant decrease of $a(T)$ as T decreases from melting induces a strongly non-uniform mechanical response within the ice sheet. Least square data correlation of Glen's (1955) laboratory data at a temperature $T_0 = 273.15$ K by Smith & Morland (1981) (hereafter referred to as SM) yielded accurate polynomial representations

$$\mathrm{SM}: \quad a_0\psi(J) = 0.3336 + 0.32J + 0.029\,63J^2, \tag{2.11}$$

where

$$a_0 = a(T_0), \quad \sigma_0 = 10^5\ \mathrm{N\ m^{-2}}, \quad D_0 = 1\ \mathrm{yr^{-1}} = 3.7 \times 10^{-8}\ \mathrm{s^{-1}}. \tag{2.12}$$

An earlier polynomial representation of the same data was given by Lliboutry (1969), but without error estimates. Note, however, that to achieve steady viscous flow on laboratory time scales, the stress levels are σ_0 and greater, and data at lower stresses are unlikely to represent a viscous response. Colbeck & Evans (1973) (hereafter referred to as CE) proposed from low stress data the representation

$$\mathrm{CE}: \quad a_0\psi(J) = 0.316 + 0.6304J + 0.743\,04J^2. \tag{2.13}$$

Both representations are used, and compared, in example solutions. The popular power law (Glen 1955) with exponent $n > 1$ implies unbounded viscosity at zero stress, with consequent artificial singularities in the reduced model. With no firm physical basis for unbounded viscosity, nor realistic laboratory data at very low stress, the analysis and examples are restricted to bounded viscosity laws. Each of these nonlinear $\psi(J)$ exhibit increasing ψ with increase of shear stress, which implies decreasing instantaneous viscosity with increase of stress. A Newtonian fluid response is described by constant $\psi(J)$ and constant $a(T)$.

The rate factor $a(T)$ has been derived by Smith & Morland (1981), using a least-squares correlation with Mellor & Testa's (1969) data over a temperature range

212–273 K, embracing the temperature range arising in natural ice sheets, at a uniaxial stress 1.18×10^6 N m^{-2} which allows the viscous response to be attained. A close correlation is obtained with a two-exponential term representation, which to an adequate approximation has the simplified form

$$a(T) = a_0 \bar{a}(\bar{T}), \quad \bar{a}(\bar{T}) = 0.68\mathrm{e}^{12\bar{T}} + 0.32\mathrm{e}^{3\bar{T}}, \tag{2.14}$$

where

$$\bar{T} = (T - T_0)/\Delta_T, \quad \Delta_T = 20\ K, \tag{2.15}$$

which will be used in examples. Note that $\bar{a}$ decreases from 1 to 1.6×10^{-2} between T_0 and $T_0 - 20$ K, and to 7.9×10^{-4} at $T_0 - 40$ K, showing the strong influence of temperature on the viscous response. An Arrhenius relation, founded in low temperature physics inappropriate to the near melting point temperature of ice masses, offers no empirical correlation when used with a single activation energy constant.

Let $(\boldsymbol{s}, \boldsymbol{j}, \boldsymbol{n})$ denote a right-hand system of unit vectors tangent and normal to the surface $z = h(r, t)$, with $\boldsymbol{s}$ having a positive radial component, then

$$\boldsymbol{s} = \Delta_h^{-1} \left(1, 0, \frac{\partial h}{\partial r}\right), \tag{2.16a}$$

$$\boldsymbol{n} = \Delta_h^{-1} \left(-\frac{\partial h}{\partial r}, 0, 1\right), \tag{2.16b}$$

where

$$\Delta_h = \left\{1 + \left(\frac{\partial h}{\partial r}\right)^2\right\}^{1/2}. \tag{2.17}$$

The vanishing of normal and tangential surface tractions t_n, t_s relative to the uniform atmospheric pressure, recognizing that the momentum jump associated with this very slow moving non-material surface is negligible, are given by

$$z = h : \left\{ \begin{array}{l} \Delta_h^2 t_\mathrm{n} = \sigma_{zz} - 2\sigma_{rz}\dfrac{\partial h}{\partial r} + \sigma_{rr}\left(\dfrac{\partial h}{\partial r}\right)^2 = 0, \\ \Delta_h^2 t_\mathrm{s} = (\sigma_{rr} - \sigma_{zz})\dfrac{\partial h}{\partial r} + \sigma_{rz}\left[1 - \left(\dfrac{\partial h}{\partial r}\right)^2\right] = 0. \end{array} \right\} \tag{2.18}$$

The normal speed u_n of the surface $z - h(r, t) = 0$ is given by

$$\frac{\partial h}{\partial t} - u_\mathrm{n}\boldsymbol{n} \cdot \nabla(z - h) = 0 \quad \Rightarrow u_\mathrm{n} = \Delta_h^{1-}\frac{\partial h}{\partial t}, \tag{2.19}$$

when $\boldsymbol{n}$ is eliminated by (2.16 b), and if q is the accumulation—the volume flux of ice entering the sheet per unit surface area per unit time—and $v_\mathrm{n} = \boldsymbol{v} \cdot \boldsymbol{n}$ is the ice particle velocity normal to the surface, then

$$q = u_\mathrm{n} - v_\mathrm{n}. \tag{2.20}$$

During surface accumulation (snowfall) q is positive, and during ablation (melting) q is negative. Strictly, q is determined by a complex interaction between the sheet and atmosphere, but here is viewed as a prescribed quantity, depending on r, t and h in general. With $\boldsymbol{n}$ given by (2.16 b) and u_n by (2.19), the surface accumulation condition (2.20), a kinematic condition, becomes

$$z = h : \quad \frac{\partial h}{\partial t} + v_r\frac{\partial h}{\partial r} - v_z = \Delta_h q, \tag{2.21}$$

which is the additional relation required to determine the unknown $h(r,t)$. The surface conditions will be completed by a prescription of surface temperature

$$z = h: \quad T = T_h, \tag{2.22}$$

given in general as a function of r, t and h; again a common simplification of thermal interaction with the atmosphere.

At the prescribed rigid bed $z = f(r)$, a right-hand system of unit vectors $(\boldsymbol{s}, \boldsymbol{j}, \boldsymbol{n})$ tangent and normal to the base of the ice sheet, with $\boldsymbol{n}$ pointing out of the sheet and $\boldsymbol{s}$ having a negative radial component, is defined by

$$\boldsymbol{s} = \Delta_f^{-1}\left(-1, 0, -\frac{\mathrm{d}f}{\mathrm{d}r}\right), \tag{2.23a}$$

$$\boldsymbol{n} = \Delta_f^{-1}\left(\frac{\mathrm{d}f}{\mathrm{d}r}, 0, -1\right), \tag{2.23b}$$

where

$$\Delta_f = \left\{1 + \left(\frac{\mathrm{d}f}{\mathrm{d}r}\right)^2\right\}^{1/2}. \tag{2.24}$$

If b is the basal drainage flux—the volume flux of ice leaving the sheet per unit surface area per unit time—positive and negative for melting and refreezing, respectively, and $v_\mathrm{n} = \boldsymbol{v}\cdot\boldsymbol{n}$ is the normal ice particle velocity normal to the bed, then

$$b = v_\mathrm{n}, \tag{2.25}$$

since the base is stationary, which, with $\boldsymbol{n}$ given by (2.23 *b*), becomes a kinematic condition

$$z = f: \quad v_r\frac{\mathrm{d}f}{\mathrm{d}r} - v_z = \Delta_f b. \tag{2.26}$$

This is not an extra condition, but replaces a normal traction prescription which is an unknown constraint stress in the rigid bed. Two forms of tangential conditions are considered. First is a non-slip limit situation appropriate to cold ice adhering everywhere to the bed for which the tangential velocity of the ice is zero,

$$z = f \text{ (non-slip)}: \quad -\Delta_f v_\mathrm{s} = v_r + v_z\frac{\mathrm{d}f}{\mathrm{d}r} = 0. \tag{2.27}$$

Second is a sliding law relating the tangential traction t_s and velocity v_s on the bed, here linearly, with a friction coefficient depending on the normal pressure $p_\mathrm{n} = -t_\mathrm{n}$. It is physically sensible to suppose that the sliding resistance becomes zero when the normal pressure vanishes, and following Morland & Johnson (1980) it is assumed that the friction coefficient is linear in p_n as $p_\mathrm{n} \to 0$, which is sufficient, and necessary, to ensure a bounded surface slope at the margin in the reduced model. That is,

$$z = f \text{ (sliding)}: \quad -t_\mathrm{s} = p_\mathrm{n}\Omega(p_\mathrm{n})v_\mathrm{s}, \quad \Omega > 0, \tag{2.28}$$

where the coefficient $\Omega(p_\mathrm{n})$ allows a nonlinear dependence on the normal bed pressure for finite p_n. The tangential and normal tractions on the bed are given by

$$\Delta_f^2 t_\mathrm{s} = (\sigma_{zz} - \sigma_{rr})\frac{\mathrm{d}f}{\mathrm{d}r} + \sigma_{rz}\left[1 - \left(\frac{\mathrm{d}f}{\mathrm{d}r}\right)^2\right], \quad \Delta_f^2 p_\mathrm{n} = -\sigma_{zz} + 2\sigma_{rz}\frac{\mathrm{d}f}{\mathrm{d}r} - \sigma_{rr}\left(\frac{\mathrm{d}f}{\mathrm{d}r}\right)^2. \tag{2.29}$$

Note that the traction of the bed on the ice resists the sliding. The actual resistance

may depend also on temperature, though this is unlikely to be important in regions of cold ice, and also on effective pressure instead of p_n, if pore water pressures in the bed are significant. Such bed hydrology is not treated here.

It is common to prescribe a vertically upward geothermal heat flux $G = 4 \times 10^{-2}\,\mathrm{N\,m^{-1}\,s^{-1}}$ ($\mathrm{W\,m^{-2}}$) arriving at the base, with the assumption that the normal flux is continuous with that in the ice. This assumption, however, is not in general a valid approximation to the energy jump condition across the ice sheet base. While the kinetic energy jump is negligible, both the internal energy jump (latent heat) and traction work contributions may be significant. Let $\boldsymbol{k}$ denote a unit vector parallel to $0z$ and let L be the latent heat of ice melt, $3.3 \times 10^5\,\mathrm{J\,kg^{-1}}$, then neglecting the kinetic energy jump and assuming traction continuity, the energy jump becomes

$$z = f: \quad \lambda \frac{\partial T}{\partial n} = -G\boldsymbol{k}\cdot\boldsymbol{n} - \rho b L + p_n b - t_s v_s. \tag{2.30}$$

The first two terms are the heat flux at the base in the ice and bed, respectively, the third term is the latent heat lost or gained as ice melts ($b > 0$) or water freezes ($b < 0$) and the last two terms are the pressure and shear traction working jumps. If b has a magnitude $q_0 = 1\,\mathrm{m\,yr^{-1}} = 3.17 \times 10^{-8}\,\mathrm{ms^{-1}}$ in melt zones near the margin, then $\rho b L$ has magnitude $10\,\mathrm{N\,m^{-1}\,s^{-1}}$, which far exceeds G, and in fact the latent heat term is only negligible when $|b| \ll 10^{-10}\,\mathrm{m\,s^{-1}}$ which may be appropriate in cold central zones. The normal pressure p_n has magnitude $\rho g h \approx 4 \times 10^7\,\mathrm{N\,m^{-2}}$ at ice thickness 4000 m, a factor 10 less than ρL, so the normal pressure working may also be negligible in a cold central zone. The tangential working is zero for non-slip, appropriate to cold central zones, but if $|t_s|$ reaches a magnitude $10^5\,\mathrm{N\,m^{-2}}$ in a zone of moderate sliding velocity v_s of order $10^{-7}\,\mathrm{m\,s^{-1}}$, then the tangential traction working is comparable to G. In cold central zones, the dominant contribution to the ice heat flux may indeed be the geothermal heat flux, but nearer the margin the latent heat contribution could be dominant if melting is significant, and there is no approximation of (2.30) satisfactory for the entire base. Whenever $b \neq 0$, the flux condition (2.30) is a relation for b coupled with the kinematic condition (2.26), and temperature is prescribed as the melting/freezing point, depending on pressure. For temperatures below the melting point, $b = 0$ and (2.30) defines the flux; that is, there are different thermal boundary conditions in the different zones. The examples presented here are for a prescribed flux uncoupled from latent heat and working contributions.

This completes the description of an idealized thermomechanically coupled radially symmetric ice sheet flow. In the steady flow limit the local heating term $\partial T/\partial t$ in the energy balance (2.7), and the rate of surface elevation change $\partial h/\partial t$ in the kinematic condition (2.21), are absent.

3. Reduced model

As discussed earlier, a substantial simplification is achieved when gradients in a longitudinal (here radial) direction are negligible compared to those in the thickness (here vertical) direction. A systematic approximation is obtained in terms of dimensionless stretched coordinates and variables defined by

$$z = d_0 Z, \quad r = \varepsilon^{-1} d_0 R, \quad h = d_0 H, \quad f = d_0 F, \quad t = d_0 \bar{t}/q_0, \tag{3.1}$$

$$v_z = q_0 W, \quad v_r = \varepsilon^{-1} q_0 U, \quad q = q_0 Q, \quad b = q_0 B, \tag{3.2}$$

$$(\boldsymbol{\sigma}, p, \hat{\boldsymbol{\sigma}}) = \rho g d_0 (\bar{\boldsymbol{\sigma}}, \bar{p}, \bar{\boldsymbol{\sigma}}), \tag{3.3}$$

where the dimensionless parameter $\varepsilon \ll 1$, and it is supposed that derivatives in R, Z and $\bar{t}$ have the same status. The vertical length and velocity scales d_0 and q_0, and time scale d_0/q_0, are chosen to ensure that Z and W are order unity, and that the time derivatives in the transformed (2.7) and (2.21) remain leading-order contributions. Thus d_0 is the ice sheet thickness magnitude, q_0 is a surface accumulation magnitude. Typical, or mean, values are

$$d_0 = 2000\,\mathrm{m}, \quad q_0 = 1\,\mathrm{m\,yr^{-1}} = 3.17\times10^{-8}\,\mathrm{m\,s^{-1}}, \quad d_0/q_0 = 2000\,\mathrm{yr} = 6.31\times10^{10}\,\mathrm{s}. \tag{3.4}$$

By construction r/d_0 and v_r/q_0 are of order ε^{-1} when R and U are of order unity, and all terms of the mass conservation (2.4) have equal status, thus

$$\frac{\partial U}{\partial R} + \frac{U}{R} + \frac{\partial W}{\partial Z} = 0. \tag{3.5}$$

The stress unit

$$\rho g d_0 = 1.801 \times 10^7\,\mathrm{N\,m^{-2}} = 180\,\mathrm{Pa} \tag{3.6}$$

is the magnitude of the overburden pressure at depth d_0, but magnitudes of the deviatoric stress components are not normalized and are given by the viscous relations.

The surface and bed slopes are

$$\frac{\partial h}{\partial r} = \varepsilon \frac{\partial H}{\partial R} = \varepsilon \Gamma, \quad \frac{\mathrm{d}f}{\mathrm{d}r} = \varepsilon \frac{\mathrm{d}F}{\mathrm{d}R} = \varepsilon \beta, \tag{3.7}$$

where Γ and β are order unity, or less, by assertion, and $\partial h/\partial r$ and $\mathrm{d}f/\mathrm{d}r$ are order ε; that is, the scaling and expansion scheme is valid only for bed slopes of order ε or less. Finite bed slope of order unity would imply β of order ε^{-1} and the following approximations fail. It now follows that to leading order in ε, neglecting terms of order ε compared to unity,

$$\Delta_h = 1, \quad \Delta_f = 1, \tag{3.8}$$

and, to leading order, the kinematic conditions (2.21) and (2.26) become

$$Z = H: \quad \frac{\partial H}{\partial \bar{t}} + U\frac{\partial H}{\partial R} - W = Q, \tag{3.9}$$

$$Z = F: \quad U\frac{\mathrm{d}F}{\mathrm{d}R} - W = B, \tag{3.10}$$

and the tangential conditions (2.27) and (2.28) become

$$Z = F \text{ (non-slip)}: \quad U = 0, \tag{3.11}$$

$$Z = F \text{ (sliding)}: \quad \bar{t}_\mathrm{s} = \bar{p}_\mathrm{n}\bar{\Omega}(\bar{p}_\mathrm{n})\varepsilon U, \tag{3.12}$$

where $t_\mathrm{s} = \rho g d_0 \bar{t}_\mathrm{s}$ according to the stress scaling (3.3), $v_\mathrm{s} = -v_r$ to leading order, and

$$\bar{\Omega}(\bar{p}_\mathrm{n}) = \Omega(\rho g d_0 \bar{p}_\mathrm{n}) > 0. \tag{3.13}$$

The surface temperature prescription (2.22) and basal heat flux condition (2.30), viewing G as a prescribed flux in the ice, uncoupled from latent heat and stress working, become

$$Z = H: \quad \bar{T} = \bar{T}_H, \tag{3.14}$$

$$Z = F: \quad \frac{\partial \bar{T}}{\partial Z} = \frac{d_0}{\lambda \Delta_T} G. \tag{3.15}$$

Leading order approximations for the basal traction (2.29) and surface tractions (2.18) depend on those for the stress components.

Asymptotic expansions in ε of the equilibrium equations, stress boundary conditions and inverted viscous relations, allowing for the significant non-uniformity introduced by $\bar{a}(\bar{T})$ (Morland 1984) show that, to leading order,

$$\bar{\sigma}_{rr} = \bar{\sigma}_{\theta\theta} = \bar{\sigma}_{zz} = -p = -(H - Z), \tag{3.16}$$

$$\bar{\sigma}_{rz} = -\varepsilon\Gamma(H - Z), \tag{3.17}$$

$$\bar{\sigma}_{rr} - \bar{\sigma}_{\theta\theta}, \quad \bar{\sigma}_{rr} - \bar{\sigma}_{zz} = O(\varepsilon^2), \tag{3.18}$$

where symmetry ensures that the equilibrium terms with factor r^{-1} remain bounded as $r \to 0$. The dominant deviatoric stress is therefore $\bar{\sigma}_{rz}$, of order ε, and, to leading order, the invariant (2.10) becomes

$$J = \left(\frac{\rho g d_0}{\sigma_0}\right)^2 \bar{\sigma}_{rz}^2 = \left(\frac{\rho g d_0 \varepsilon}{\sigma_0}\right)^2 \Gamma^2 (H - Z)^2, \tag{3.19}$$

while the corresponding dominant strain-rate becomes

$$D_{rz} = \frac{\varepsilon^{-1} q_0}{2 d_0} \frac{\partial U}{\partial Z}. \tag{3.20}$$

Hence the viscous relation (2.9) now yields an order unity balance

$$\frac{\partial U}{\partial Z} = -2\bar{a}(\bar{T})\psi(J)\Gamma(H - Z) \tag{3.21}$$

by choosing

$$\varepsilon = \left\{\frac{\sigma_0 q_0}{\rho g d_0^2 D_0 a_0}\right\}^{1/2} \tag{3.22}$$

and

$$J = \vartheta \Gamma^2 (H - Z)^2, \quad \vartheta = \frac{\rho g q_0}{\sigma_0 D_0 a_0}. \tag{3.23}$$

With the values (2.12) and (3.4), and choosing the factor $a_0 = 1$ to equate laboratory ice response with the natural ice response,

$$\varepsilon = 0.001\,66, \quad \vartheta = 0.09. \tag{3.24}$$

Define

$$\tau = \zeta \varepsilon^{-1} \bar{\sigma}_{rz} = -\zeta \Gamma (H - Z), \tag{3.25a}$$

$$\zeta = -\operatorname{sgn}(\Gamma), \tag{3.25b}$$

so that $\zeta = \pm 1$ for $\Gamma \lessgtr 0$, and $\tau \geqslant 0$ everywhere, then

$$\frac{\partial U}{\partial Z} = \zeta \bar{a}(\bar{T}) g(\tau), \tag{3.26}$$

where

$$g(\tau) = 2\tau\psi(\vartheta\tau^2) \geqslant 0, \quad g'(\tau) > 0, \tag{3.27}$$

and a prime denotes differentiation with respect to argument. Note that $\bar{\sigma}_{rz}$ and $\partial U/\partial Z$ have the sign of ζ; that is, of $-\Gamma$ at the given R for all Z. Inclusion of ζ allows the surface slope Γ to change sign along the profile, while retaining the

positive function $g(\tau)$ with the positive argument τ. The sliding law (3.12), (3.13) becomes

$$Z = F: \quad \zeta\tau_{\rm b} = \bar{p}_{\rm b}\bar{\Omega}(\bar{p}_{\rm b})U_{\rm b}, \tag{3.28}$$

where $\tau_{\rm b}$, $\bar{p}_{\rm b}$ and $U_{\rm b}$ are values on the bed, so

$$\zeta\tau_{\rm b} = -\Gamma(H-F), \tag{3.29a}$$

$$\bar{p}_{\rm b} = H - F. \tag{3.29b}$$

Corresponding to the polynomial laws (2.11) and (2.13),

$$\text{SM}: \quad g(\tau) = 0.6672\tau + 0.05764\tau^3 + 0.00048\tau^5, \tag{3.30}$$

$$\text{CE}: \quad g(\tau) = 0.632\tau + 0.11355\tau^3 + 0.012052\tau^5, \tag{3.31}$$

and $g(\tau) \sim \tau$ as $\tau \to 0$. The energy balance (2.7) becomes

$$\frac{\partial\bar{T}}{\partial\bar{t}} + U\frac{\partial\bar{T}}{\partial R} + W\frac{\partial\bar{T}}{\partial Z} = k\frac{\partial^2\bar{T}}{\partial Z^2} + \alpha\bar{a}(\bar{T})\tau g(\tau) + \bar{s}, \tag{3.32}$$

where

$$k = \frac{\lambda}{\rho C d_0 q_0}, \quad \alpha = \frac{g d_0}{C\Delta_T}, \quad \bar{s} = \frac{s d_0}{\rho C \Delta_T q_0}. \tag{3.33}$$

Here

$$k = 0.0189, \quad \alpha = 0.491. \tag{3.34}$$

The thermomechanically coupled reduced model is the energy balance (3.32), mass balance (3.5) and viscous relation (3.26), subject to the thermal boundary conditions (3.14), (3.15), the kinematic conditions (3.9), (3.10), and basal tangential condition (3.11) or (3.28), to determine U, W and $\bar{T}$, and $H(R,\bar{t})$, and then leading order stresses are given by (3.16) and (3.17).

4. Prescribed temperature theory

If the temperature field $\bar{T}(R,Z,\bar{t})$ is prescribed, and hence $\bar{a}(\bar{T}) = \tilde{a}(R,Z,\bar{t})$ is prescribed, then the viscous relation (3.26) may be formally integrated to express U in terms of H and Γ, and then the mass balance (3.5) solved to derive W in terms of H and Γ. Once this has been done, the kinematic conditions (3.9) and (3.10) combine to yield a parabolic equation for $H(R,\bar{t})$ of stable diffusion form. This has been demonstrated in the plane flow case by Morland (1984), following the formulation of an ordinary differential equation for $H(X)$ in steady plane flow by Morland & Smith (1984). Before the analogous radial flow analysis is presented, consider the implications for the coupled theory. The prescribed temperature field can satisfy prescribed boundary conditions (3.14) and (3.15), and can echo an expected qualitative behaviour based on core data, but will not satisfy the energy balance (3.32). This simpler theory is therefore directly useful for investigating the qualitative effects of plausible temperature distributions through an ice sheet, which will be exploited in later examples, but also serves as a valuable test bed for direct numerical algorithms constructed for the coupled equations. By including an algebraic source term

$$\bar{s} = \frac{\partial\bar{T}}{\partial\bar{t}} + U\frac{\partial\bar{T}}{\partial R} + W\frac{\partial\bar{T}}{\partial Z} - k\frac{\partial^2\bar{T}}{\partial Z^2} \tag{4.1}$$

in the coupled reduced energy balance, determined by the prescribed $\bar{T}$, and setting $\alpha = 0$ in the direct computation, the temperature, velocity and stress fields are the

same for both solutions. More generally, a full coupled equations algorithm can also be tested when the bed form has small (order ε) slope. The steady flow solutions presented later are therefore tests for the full steady flow algorithm, but are also tests for the unsteady flow algorithm, since an incorrect evolution calculation will not approach a correct steady limit.

The mass balance (3.5) is satisfied identically by velocity components

$$U = \frac{1}{R}\frac{\partial \omega}{\partial Z}, \tag{4.2a}$$

$$W = -\frac{1}{R}\frac{\partial \omega}{\partial R} \tag{4.2b}$$

in terms of a stream function $\omega(R, Z, \bar{t})$. The kinematic conditions (3.9) and (3.10) are now expressed by

$$\frac{\partial H}{\partial \bar{t}} + \frac{1}{R}\frac{\partial}{\partial R}\{\omega[R, H(R, \bar{t}), \bar{t}]\} = Q, \tag{4.3}$$

$$\frac{1}{R}\frac{\partial}{\partial R}\{\omega[R, F(R), \bar{t}]\} = B. \tag{4.4}$$

Define

$$g_1(R, Z, \bar{t}) = \int_F^Z \bar{a}(\bar{T}')g(\tau')\,\mathrm{d}Z', \tag{4.5}$$

where

$$\bar{T}' = \bar{T}(R, Z', \bar{t}), \quad \tau' = -\zeta\Gamma(H - Z'), \tag{4.6}$$

and

$$g_2(R, Z, \bar{t}) = \int_F^Z g_1(R, Z', \bar{t})\,\mathrm{d}Z'. \tag{4.7}$$

The prime is introduced to indicate a running integration variable. Now, by (3.26),

$$U(R, Z, \bar{t}) = U_\mathrm{b}(R, \bar{t}) + \zeta g_1(R, Z, \bar{t}), \tag{4.8}$$

which is identically zero on $R = 0$, since U_b, τ and hence g, are zero on $R = 0$, and then by (4.2 a),

$$\omega(R, Z, \bar{t}) = \omega(R, F, \bar{t}) + RU_\mathrm{b}(R, \bar{t})[Z - F] + R\zeta g_2(R, Z, \bar{t}), \tag{4.9}$$

noting that $g_1(R, F, \bar{t}) = g_2(R, F, \bar{t}) = 0$ by construction. Differencing (4.3) and (4.4), with $\omega(R, H, \bar{t}) - \omega(R, F, \bar{t})$ expressed by (4.9), yields the parabolic differential equation

$$\frac{\partial H}{\partial \bar{t}} + \frac{1}{R}\frac{\partial}{\partial R}\{R[H(R) - F(R)]U_\mathrm{b}(R, \bar{t}) + \zeta R g_2[R, H(R, \bar{t}), \bar{t}]\} = Q - B = Q^*, \tag{4.10}$$

for $H(R, \bar{t})$, where U_b is zero for non-slip or is given by the sliding law (3.28) in terms of Γ and H.

The spatial operator in (4.10) is second order, since g_2, and U_b with sliding, depend on $\Gamma = \partial H/\partial R$, and a stable diffusion form requires the coefficient of $\partial^2 H/\partial R^2$ to be negative. The complete operator is now constructed since it is required in later solution constructions. Introduce the thickness $\Delta(R, \bar{t})$ defined by

$$\Delta = H - F, \tag{4.11}$$

then the basal stresses and sliding law (3.29), (3.28) can be written

$$\bar{p}_\mathrm{b} = \Delta, \quad \zeta\tau_\mathrm{b} = -\Gamma\Delta = \Delta\bar{\Omega}(\Delta)U_\mathrm{b}. \tag{4.12}$$

The symbols Δ_T, Δ_h and Δ_f defined in (2.15), (2.17) and (2.24) no longer appear in the analysis. With the sliding law (4.12), (4.10) becomes

$$\frac{\partial H}{\partial \bar{t}} + R^{-1}\left\{\zeta g_2[\,] - \frac{\Gamma\Delta}{\bar{\Omega})(\Delta)}\right\} + \frac{\partial}{\partial R}\left\{\zeta g_2[\,] - \frac{\Gamma\Delta}{\bar{\Omega}(\Delta)}\right\} = Q^*, \tag{4.13}$$

where $g_2[\,]$ denotes $g_2[R, H(R,\bar{t}),\bar{t}]$. For non-slip only the $g_2[\,]$ terms appear in the $\{\}$ terms, corresponding to $\bar{\Omega}^{-1} = 0$. Interchanging the order of integration in the repeated integrals formed by (4.7) and (4.5) gives

$$g_2(R, Z, \bar{t}\,) = \int_F^Z (Z - Z')\bar{a}(\bar{T}')g(\tau')\,\mathrm{d}Z', \tag{4.14}$$

and in particular

$$g_2[R, H(R,\bar{t}\,),\bar{t}\,] = \int_F^H (H - Z)\bar{a}(\bar{T})g(\tau)\,\mathrm{d}Z, \tag{4.15}$$

Now introduce a change of variable

$$H - Z = \Delta y, \quad 0 \leqslant y \leqslant 1, \tag{4.16}$$

where $y = 0$ and $y = 1$ denote the surface and bed, respectively; then by (3.25 *a*), (3.29 *a*), (4.11) and (4.15),

$$\tau = \tau_\mathrm{b} y, \quad \frac{\partial \tau_\mathrm{b}}{\partial R} = -\zeta\left\{\Delta\frac{\partial^2 H}{\partial R^2} + \Gamma(\Gamma - \beta)\right\} \tag{4.17}$$

and

$$g_2[\,] = \Delta^2 \int_0^1 \bar{a}(\bar{T})g(\tau_\mathrm{b} y)y\,\mathrm{d}y. \tag{4.18}$$

General temperature and net accumulation prescriptions can be expressed in the forms

$$T = \tilde{T}(R, \Delta, y, \bar{t}, R_\mathrm{M}), \tag{4.19 *a*}$$

$$Q^* = \tilde{Q}(R, \Delta, y, \bar{t}, R_\mathrm{M}), \tag{4.19 *b*}$$

where R_M is the (unknown) margin radius. Then

$$\left.\frac{\partial T}{\partial R}\right|_y = \frac{\partial \tilde{T}}{\partial R} + \frac{\partial \tilde{T}}{\partial \Delta}(\Gamma - \beta). \tag{4.20}$$

Define

$$I = \int_0^1 \bar{a}(\bar{T})g(\tau_\mathrm{b} y)y\,\mathrm{d}y, \tag{4.21}$$

$$J = \int_0^1 \bar{a}(\bar{T})g'(\tau_\mathrm{b} y)y^2\,\mathrm{d}y, \tag{4.22}$$

$$K_R = \int_0^1 \bar{a}'(\bar{T})g(\tau_\mathrm{b} y)y\frac{\partial \tilde{T}}{\partial R}\,\mathrm{d}y, \tag{4.23}$$

$$K_D = \int_0^1 \bar{a}'(\bar{T})g(\tau_\mathrm{b} y)y\frac{\partial \tilde{T}}{\partial \Delta}\,\mathrm{d}y, \tag{4.24}$$

where the integrals I, J, K_R, K_D are functions of R, Δ, Γ, $\bar{t}$ and $R_{\rm M}$, and I and J are strictly positive. Thus, the radial derivatives required in (4.13) are

$$\zeta\frac{\partial g_2[\,]}{\partial R} = 2\zeta I\Delta(\Gamma-\beta) - J\Delta^2\left\{\Delta\frac{\partial^2 H}{\partial R^2} + \Gamma(\Gamma-\beta)\right\} + \zeta\Delta^2\{K_R + K_D(\Gamma-\beta)\}, \quad (4.25)$$

and

$$-\frac{\partial}{\partial R}\left\{\frac{\Gamma\Delta}{\bar{\Omega}(\Delta)}\right\} = -\frac{\Delta}{\bar{\Omega}}\frac{\partial^2 H}{\partial R^2} - \frac{\Gamma(\Gamma-\beta)}{\bar{\Omega}} + \frac{\Gamma\Delta(\Gamma-\beta)\bar{\Omega}'}{\bar{\Omega}^2}. \quad (4.26)$$

With the definitions (4.21)–(4.24) and derivatives (4.25) and (4.26), the profile equation (4.13) becomes

$$\frac{\partial H}{\partial \bar{t}} - \left\{J\Delta^3 + \frac{\Delta}{\bar{\Omega}}\right\}\frac{\partial^2 H}{\partial R^2} + \zeta\Delta(\Gamma-\beta)\{2I + K_D\Delta\}$$
$$-\Gamma(\Gamma-\beta)\left\{J\Delta^2 + \frac{1}{\bar{\Omega}} - \frac{\Delta\bar{\Omega}'}{\bar{\Omega}^2}\right\} + \zeta K_R\Delta^2 + \frac{1}{R}\left\{\zeta I\Delta^2 - \frac{\Gamma\Delta}{\bar{\Omega}}\right\} = Q^*. \quad (4.27)$$

The non-slip equation is obtained by setting $\bar{\Omega}^{-1} = 0$. The coefficient of $\partial^2 H/\partial R^2$ in (4.27) is $-(J\Delta^3 + \Delta/\bar{\Omega})$, which is negative as asserted. The plane flow equation corresponding to (4.27) has R replaced by a horizontal rectangular coordinate X and the term with a factor R^{-1} is absent. The explicit operator for plane flow was not presented by Morland (1984), but was given by Hindmarsh *et al.* (1987) in terms of integrals with respect to Z from F to H. Equation (4.27) can be written as a differential equation for $\Delta(R,\bar{t}\,)$, but explicitly involves $F(R)$, $F'(R)$ and $F''(R)$. The boundary conditions are

$$R = 0: \quad \frac{\partial H}{\partial R} = 0, \quad (4.28)$$

$$R = R_{\rm M}\ \text{(unknown)}: \quad \Delta = H - F = 0. \quad (4.29)$$

Once $H(R,\bar{t}\,)$ is determined, the stresses and velocities follow from (3.16), (3.17), (4.8), (4.9) and (4.2 *b*).

In steady flow, (4.27) reduces to a second-order ordinary differential equation for $H(R)$ or $\Delta(R)$, subject to the boundary conditions (4.28) and (4.29). This steady theory allows explicit determination of the bounded surface slope $\Gamma_{\rm M}$ at the margin $R_{\rm M}$ with the sliding law (4.12), and the asymptotic form of the unbounded surface slope at $R_{\rm M}$ in the case of non-slip, which in turn yield boundary-value problems for the simultaneous determination of $\Delta(R)$ and $R_{\rm M}$.

5. Steady flow

The steady flow thickness profile $\Delta(R)$ is governed by the second-order ordinary differential equation obtain from (4.10) when time dependence is absent,

$$\frac{\mathrm{d}}{\mathrm{d}R}\{R\Delta U_{\rm b} + \zeta R g_2[\,]\} = RQ^*, \quad (5.1)$$

which has a formal integral

$$\Delta U_{\rm b} + \zeta g_2[\,] = -\frac{1}{R}\int_R^{R_{\rm M}} R'Q^*\,\mathrm{d}R', \quad (5.2)$$

since $\Delta = 0$ at $R = R_{\mathrm{M}}$ and $g_2[\ ]$ evaluated at $H = F$ is zero by construction. If Q^* is given as a function of R or the distance from the margin, $R - R_{\mathrm{M}}$, then the integral in (5.2) can be evaluated explicitly. Since the integral (4.18) for $g_2[\ ]$ and the sliding relation (4.12) for U_{b} depend only on Δ and $\Gamma = \Delta' + \beta$, (5.2) is then in general a first-order integro-differential equation for $\Delta(R)$ which, in special cases (Appendix B), can be solved analytically to generate test problems for the numerical algorithm constructed for the second-order equation. For a general Q^* prescription of the form (4.19*b*), the integral property (5.2) can be verified at each step of the differential equation solution to compare validity and accuracy of the algorithm.

First consider the non-slip case $U_{\mathrm{b}} \equiv 0$. Recall that $g(\tau) \sim \tau$ as $\tau \to 0$ by (3.27), since $\psi(0) > 0$, so if Γ is bounded as $R \to R_{\mathrm{M}}$ and $\Delta \to 0$, then by the definition of τ_{b} (4.12), $\tau_{\mathrm{b}} \sim \Delta$ and then by (4.18), $g_2[\ ] \sim \Delta^3$. Let $Q \to Q_{\mathrm{M}}$ smoothly in R as $R \to R_{\mathrm{M}}$, then the integral term in (5.2) $\sim -Q_{\mathrm{M}}(R_{\mathrm{M}} - R)$ as $R \to R_{\mathrm{M}}$. For a steady profile, it is reasonable to assert that there is net melting at the margin, so that $Q^*_{\mathrm{M}} < 0$. Thus (5.2) implies that $\Delta^3 \sim (R_{\mathrm{M}} - R)$ and hence $\Delta'(R) \sim (R_{\mathrm{M}} - R)^{-2/3}$ is unbounded, contradicting the supposition of bounded Γ. Thus Γ must be unbounded at the margin. This contradicts the validity requirement of the reduced model that Γ is order unity, but non-slip will be treated as a mathematical limit case recognizing that the solution does not approximate the flow near the margin, and perhaps elsewhere. Now allow unbounded Γ, hence unbounded Δ', but since $g_2[\ ]$ is bounded by (5.2), then g must be bounded and hence τ_{b} remains bounded. Let $\tau_{\mathrm{b}} \to \tau_{\mathrm{M}}$ smoothly in R as $R \to R_{\mathrm{M}}$, where τ_{M} is the finite margin traction, positive by definition. Then, since $\Gamma \sim \Delta'$ as $R \to R_{\mathrm{M}}$ because β is bounded, by the expression (3.29) for τ_{b},

$$-\zeta \Delta \Delta' = -\tfrac{1}{2}\zeta(\Delta^2)' \sim \tau_{\mathrm{M}} \quad \text{as } R \to R_{\mathrm{M}}, \tag{5.3}$$

from which $\zeta_{\mathrm{M}} = +1$ and hence

$$\Delta \sim (2\tau_{\mathrm{M}})^{1/2}(R_{\mathrm{M}} - R)^{1/2}, \tag{5.4a}$$

$$\Delta' \sim -\tfrac{1}{2}(2\tau_{\mathrm{M}})^{1/2}(R_{\mathrm{M}} - R)^{-1/2}, \tag{5.4b}$$

$$\Delta'' \sim -\tfrac{1}{4}(2\tau_{\mathrm{M}})^{1/2}(R_{\mathrm{M}} - R)^{-3/2}. \tag{5.4c}$$

The surface necessarily slopes down to the bed at the margin. Let $\bar{a}(\bar{T}) \to \bar{a}_{\mathrm{M}}$ smoothly in R as $R \to R_{\mathrm{M}}$, then by (4.18) and (5.2),

$$\Delta^2 \bar{a}_{\mathrm{M}} \int_0^1 g(\tau_{\mathrm{M}} y) y \, \mathrm{d}y \sim (-Q^*_{\mathrm{M}})(R_{\mathrm{M}} - R), \tag{5.5}$$

and replacing Δ^2 by the asymptotic form (5.4*a*) shows that

$$\tau_{\mathrm{M}} \int_0^1 g(\tau_{\mathrm{M}} y) y \, \mathrm{d}y = \frac{-Q^*_{\mathrm{M}}}{2\bar{a}_{\mathrm{M}}} > 0. \tag{5.6}$$

Since g and g' are positive, the left-hand side of (5.6) is a monotonic increasing function of τ_{M}, zero at $\tau_{\mathrm{M}} = 0$, and hence determines a unique positive root τ_{M} when $Q^*_{\mathrm{M}} < 0$ as proposed. If $Q^*_{\mathrm{M}} > 0$, there can be no solution.

For numerical solution, bounded derivatives are more convenient and the transformation

$$R_{\mathrm{M}} - R = R_{\mathrm{M}} t^2, \quad \Delta(R) = \tilde{\Delta}(t) \tag{5.7}$$

introduces a normalized variable t (time no longer enters the analysis so the previous

definition of t is redundant) with $t = 0$ at the margin $R = R_{\rm M}$ and $t = 1$ at the divide $R = 0$. Then

$$\kappa(t) = \tilde{\Delta}'(t) = -2R_{\rm M}t\Delta'(R) = -2R_{\rm M}^{1/2}(R_{\rm M} - R)^{1/2}\Delta'(R) \tag{5.8}$$

is bounded as $R \to R_{\rm M}$. By (5.4), the limit value as $R \to R_{\rm M}$ is

$$\kappa_{\rm M} = (2R_{\rm M}\tau_{\rm M})^{1/2} > 0, \tag{5.9}$$

given as a function of the unknown $R_{\rm M}$, noting that $\tau_{\rm M}$ determined by (5.6) can also depend on $R_{\rm M}$ through $Q^*_{\rm M}$ and $\bar{a}_{\rm M}$. Further, differentiating (5.8) with respect to t,

$$\kappa'(t) = -2R_{\rm M}\{\Delta'(R) - 2(R_{\rm M} - R)\Delta''(R)\}, \tag{5.10}$$

which, by (5.4), is bounded as $t \to 0$. However, the leading-order asymptotic results (5.4) simply show that the apparent term in $(R_{\rm M} - R)^{-1/2}$ vanishes, and further terms in the expansions are required to determine the margin value of $\kappa'(t)$ which is needed in the later numerical algorithm. Thus, consider an expansion

$$\tilde{\Delta}(t) \sim \kappa_{\rm M}t(1 + \delta_{\rm N}t + \cdots) \quad \text{as } t \to 0, \tag{5.11}$$

from which $\kappa'(t) \to 2\kappa_{\rm M}\delta_{\rm N}$ as $t \to 0$. Substituting (5.11) into (5.2) leads, after some calculation (Appendix A), to the following relation for $\delta_{\rm N}$:

$$\delta_{\rm N}\{3\bar{a}_{\rm M}\tau_{\rm M}^2 c_1 - Q^*_{\rm M}\} = \bar{a}_{\rm M}\tau_{\rm M}(\kappa_{\rm M}\beta_{\rm M}c_1 - c_0) - \tfrac{1}{3}\kappa_{\rm M}\left.\frac{\partial Q}{\partial \Delta}\right|_{\rm M}, \tag{5.12}$$

where $\beta_{\rm M} = \beta(R_{\rm M})$,

$$c_1 = \int_0^1 g'(\tau_{\rm M}y)y^2\,{\rm d}y, \quad B_{\rm M}(y) = \left.\frac{\partial \bar{T}}{\partial \Delta}\right|_{\rm M}\kappa_{\rm M}, \quad c_0 = \int_0^1 g(\tau_{\rm M})y\frac{\bar{a}'(\bar{T}_{\rm M})}{a_{\rm M}}B_{\rm M}(y)\,{\rm d}y. \tag{5.13}$$

The differential equation (5.1) with $U_{\rm b} = 0$ and $g_2[\,]$ derivative (4.25), transformed by (5.7), (5.8) and (5.10), can be written (Press *et al.* 1992) as three first-order differential equations,

$$\frac{{\rm d}\tilde{\Delta}}{{\rm d}t} = \kappa, \quad \frac{{\rm d}\kappa}{{\rm d}t} = G_{\rm N}(t, \Delta, \kappa, R_{\rm M}), \quad \frac{{\rm d}R_{\rm M}}{{\rm d}t} = 0, \tag{5.14}$$

for $\tilde{\Delta}(t)$, $\kappa(t)$ and $R_{\rm M}$ subject to the two-point boundary conditions

$$\begin{aligned} t = 0: &\quad \tilde{\Delta} = 0, \quad \kappa = \kappa_{\rm M}(R_{\rm M}), \\ t = 1: &\quad \kappa = 0. \end{aligned} \tag{5.15}$$

Since $\kappa = 0$ at $t = 1$, then $\Gamma = 0$ and $\tau_{\rm b} = 0$ at $R = 0$, hence $g_2[\,] = 0$, and so the integral property (5.2) implies

$$\int_0^{R_{\rm M}} RQ^*\,{\rm d}R = 2R_{\rm M}^2\int_0^1 t(1 - t^2)Q^*\,{\rm d}t = 0, \tag{5.16}$$

which verifies that there is no net ice flux into the sheet between the divide and the margin, recalling that $U \equiv 0$ on $R = 0$. The function $G_{\rm N}$ is detailed in Appendix A, together with verification that the terms with factor R^{-1} are bounded as $R \to 0$ $(t \to 1)$, but indeterminate so that numerical integration must end at $t = 1 - \varepsilon_r$ $(0 < \varepsilon_r \ll 1)$. This algebraic form is also indeterminate at $R = R_{\rm M}$ $(t = 0)$ and is replaced by the asymptotic limit given by (5.11) and (5.12)

$$G_{\rm N}(t, \tilde{\Delta}, \kappa, R_{\rm M}) \sim 2\kappa_{\rm M}\delta_{\rm N} \quad \text{as } t \to 0. \tag{5.17}$$

A shooting-method algorithm, starting with a trial R_{M}, based on 'numerical recipes' (Press *et al.* 1992), has been constructed to solve the system (5.14), subject to the initial conditions (5.15) at $t = 0$, and the test criterion for a successful R_{M} is to require that both κ and $g_2[\,]$ vanish at $t = 1-\varepsilon_r$, by minimizing $\{\kappa^2 + I^2\}^{1/2}$, where the integral I is defined in (4.21). Various features of the algorithm have been tested, and accuracy verified, by comparison with exact solutions (discussed in Appendix B).

Next consider the case when U_{b} is given by a sliding law of the form (4.12), for which the reduced model determines a uniformly valid leading-order solution at the margin and the divide. If the $g_2[\,]$ term in (5.2) still contributes to the balance as $R \to R_{\mathrm{M}}$, then Γ is unbounded and the asymptotic relations (5.14) hold. If the U_{b} term also contributes to the balance, then $\Delta U_{\mathrm{b}} \sim (R_{\mathrm{M}} - R)$ and hence $U_{\mathrm{b}} \sim (R_{\mathrm{M}} - R)^{1/2}$, while $\tau_{\mathrm{b}} \sim \tau_{\mathrm{M}} > 0$. The sliding relation between τ_{b} and U_{b} must then have an unbounded friction coefficient as $R \to R_{\mathrm{M}}$, $\Delta \to 0$; that is, as the normal pressure becomes zero, which is not physically sensible. An acceptable sliding relation must therefore yield a ΔU_{b} behaviour which dominates the $g_2[\,]$ behaviour as $R \to R_{\mathrm{M}}$; that is, $U_{\mathrm{b}} > 0(\Delta)^2$ as $\Delta \to 0$, and the (5.2) balance requires that $\Delta U_{\mathrm{b}} \sim (R_{\mathrm{M}} - R)$ as $R \to R_{\mathrm{M}}$. A bounded margin slope $\Gamma_{\mathrm{M}} = \Delta'_{\mathrm{M}} + \beta_{\mathrm{M}}$ then requires $U_{\mathrm{b}} > 0$ at $R = R_{\mathrm{M}}$, so that

$$\Delta \sim (\beta_{\mathrm{M}} - \Gamma_{\mathrm{M}})(R_{\mathrm{M}} - R) \quad \text{as } R \to R_{\mathrm{M}}. \tag{5.18}$$

The form of sliding law (4.12), with the proportionality $t_{\mathrm{s}} \propto -p_{\mathrm{n}}$ as $p_{\mathrm{n}} \to 0$ introduced by Morland & Johnson (1980), gives $U_{\mathrm{b}} = -\bar{\Omega}^{-1}(\Delta)\Gamma$, and the balance (5.2) yields the limits $\zeta_{\mathrm{M}} = +1$ and

$$\Gamma_{\mathrm{M}}(\beta_{\mathrm{M}} - \Gamma_{\mathrm{M}}) - \bar{\Omega}(0)Q^*_{\mathrm{M}} = 0, \tag{5.19}$$

which ensures a bounded margin slope Γ_{M}. Note that, without the p_{n} proportionality, $\Delta U_{\mathrm{b}} \sim \Delta^2\Gamma$, and hence (5.2) implies that $(\Delta^3)' \sim (R_{\mathrm{M}} - R)$ and Δ' is again unbounded at the margin. Adopting (4.12) with the resulting margin balance (5.19), there are two real roots

$$\Gamma_{\mathrm{M}} = \tfrac{1}{2}\{\beta_{\mathrm{M}} \pm [\beta^2_{\mathrm{M}} - 4\bar{\Omega}(0)Q^*_{\mathrm{M}}]^{1/2}\}, \tag{5.20}$$

provided that

$$4\bar{\Omega}(0)Q^*_{\mathrm{M}} < \beta^2_{\mathrm{M}}, \tag{5.21}$$

trivially satisfied if $Q^*_{\mathrm{M}} < 0$, which reflects an expected net margin melting. Since ice thickness $\Delta(R)$ is positive for $R < R_{\mathrm{M}}$, a permitted Γ_{M} must satisfy

$$\beta_{\mathrm{M}} - \Gamma_{\mathrm{M}} > 0. \tag{5.22}$$

If $Q^*_{\mathrm{M}} > 0$, net margin accumulation, then with (5.21),

$$Q^*_{\mathrm{M}} > 0: \quad 0 < [\beta^2_{\mathrm{M}} - 4\bar{\Omega}(0)Q^*_{\mathrm{M}}]^{1/2} < |\beta_{\mathrm{M}}|, \tag{5.23}$$

and

$$\beta_{\mathrm{M}} - \Gamma_{\mathrm{M}} = \tfrac{1}{2}\{\beta_{\mathrm{M}} \mp [\beta^2_{\mathrm{M}} - 4\bar{\Omega}(0)Q^*_{\mathrm{M}}]^{1/2}\} \tag{5.24}$$

is positive for both roots if $\beta_{\mathrm{M}} > 0$, allowing two values of Γ_{M}, but negative for $\beta_{\mathrm{M}} < 0$, allowing no valid Γ_{M}. For $Q^*_{\mathrm{M}} < 0$, the second inequality of (5.23) is reversed and $\beta_{\mathrm{M}} - \Gamma_{\mathrm{M}}$ is positive only for the second root, and unique Γ_{M} is given by

$$Q^*_{\mathrm{M}} < 0: \quad \Gamma_{\mathrm{M}} = \tfrac{1}{2}\{(\beta_{\mathrm{M}} - [\beta^2_{\mathrm{M}} - 4\bar{\Omega}(0)Q^*_{\mathrm{M}}]^{1/2}\}^{1/2} < 0. \tag{5.25}$$

Similar conclusions follow for a more general dependence of v_s on t_s. In place of (4.12), consider

$$\zeta\bar{\Omega}(\Delta)U_b = S(\tau_b/\Delta), \quad S(0) = 0, \quad S' > 0, \tag{5.26}$$

which retains $\tau_b \sim -p_b$ as $p_b \to 0$, $U_b = 0$ for $\tau_b = 0$ and assumes that ζU_b increases as τ_b/p_0 increases. The (5.2) limit now becomes

$$\Phi(\Gamma_M) = (\beta_M - \Gamma_M)S(-\zeta_M\Gamma_M) + \zeta_M\bar{\Omega}(0)Q^*_M = 0, \tag{5.27}$$

where

$$\Phi(\beta_M) = \zeta_M\bar{\Omega}(0)Q^*_M, \quad \Phi(\Gamma_M) \to \infty \quad \text{as } (\Gamma_M) \to -\infty \tag{5.28}$$

and

$$\Phi'(\beta_M) = -\{S(-\zeta_M\Gamma_M) + \zeta_M(\beta_M - \Gamma_M)S'(-\zeta_M\Gamma_M)\}. \tag{5.29}$$

If $Q^*_M < 0$ and $\zeta_M = 1$ ($\Gamma_M < 0$), then $\Phi(\beta_M) < 0$ and $\Phi'(\beta_M) < 0$, and hence there is a unique negative root Γ_M satisfying (5.22), which is the analogue of (5.25). The form (5.26) allows, for example, a power law in τ_b/Δ with exponent greater than unity, the case (5.25). Johnson (1981) presented solutions for power law sliding on a flat bed for an isothermal sheet.

Since Γ, and higher derivatives, remain bounded at $R = R_M$, an appropriate transformation to normalize the range is

$$R_M - R = R_M t, \quad \Delta(R) = \tilde{\Delta}(t), \tag{5.30}$$

with $t = 0$ and $t = 1$ denoting margin and divide, respectively. Then

$$\kappa(t) = \tilde{\Delta}'(t) = -R_M\Delta'(R), \quad \kappa_M = R_M(\beta_M - \Gamma_M) > 0 \tag{5.31}$$

and, by (5.25) with the second root,

$$\kappa_M = \tfrac{1}{2}R_M\{\beta_M + [\beta^2_M - 4\bar{\Omega}(0)Q^*_M]^{1/2}\}. \tag{5.32}$$

The differential equation (5.1) with U_b, and $g_2[\,]$ derivatives (4.26) and (4.25), transform to three first-order differential equations

$$\frac{d\tilde{\Delta}}{dt} = \kappa, \quad \frac{d\kappa}{dt} = G_s(t, \Delta, \kappa, R_M), \quad \frac{dR_M}{dt} = 0, \tag{5.33}$$

for $\tilde{\Delta}(t)$, $\kappa(\tau)$, R_M subject to the two-point conditions (5.15), with κ_M here given by (5.32), depending on R_M. The function G_s is detailed in Appendix A, along with its properties as $R \to 0$ and as $R \to R_M$. The behaviour as $R \to R_M$ again requires an expansion

$$\tilde{\Delta} \sim \kappa_M t(1 + \delta_s t + \cdots) \quad \text{as } t \to 0, \tag{5.34}$$

so that

$$G_s(t, \tilde{\Delta}, \kappa, R_M) \sim 2\kappa_M\delta_s \quad \text{as } t \to 0, \tag{5.35}$$

where (Appendix A) δ_s is given by

$$\frac{2\kappa_M\delta_s}{R^2_M}\left(3 - \beta_M\frac{R_M}{\kappa_M}\right) = -\bar{\Omega}(0)\left\{\left.\frac{\partial\tilde{Q}}{\partial\Delta}\right|_M - \frac{R_M}{\kappa_M}\left.\frac{\partial\tilde{Q}}{\partial R}\right|_M\right\}$$
$$+2\frac{\bar{\Omega}'(0)}{\bar{\Omega}(0)}\left\{\left(\frac{\kappa_M}{R_M}\right)^2 - \beta_M\left(\frac{\kappa_M}{R_M}\right)\right\} - 2\beta'(R_M) - \frac{\beta_M}{R_M} + \frac{\kappa_M}{R^2_M}, \tag{5.36}$$

recalling the definition (4.19) of $\tilde{Q}$. The integral property (5.2) implies that

$$\int_0^{R_M} RQ^* \, \mathrm{d}R = R_M^2 \int_0^1 (1-t)Q^* \, \mathrm{d}t = 0. \tag{5.37}$$

The numerical algorithm is discussed in Appendix B.

6. Illustrations

A variety of examples have been computed to illustrate the influences of the viscous law $g(\tau)$, specifically the polynomial representations (3.30) (Smith & Morland 1981) and (3.31) (Colbeck & Evans 1973) correlated with different data sets, the prescribed temperature distribution $\bar{t}$, the net accumulation function Q^*, and the bed form $F(R)$, and the contrast between non-slip and a linear sliding law (4.12) on the bed. Selected solutions with the evaluated heat source $\bar{s}$ will provide valuable validity and accuracy tests for direct numerical treatments of the thermomechanically coupled reduced system in steady state, or the steady limit of evolutionary solutions, and also for the full (non-reduced) system when the bed form is flat or has very low slopes.

The first set of examples compared two accumulation distributions, two temperature distributions, a flat bed, a bed with a hump and a bed with a basin, for both viscous laws (Smith & Morland 1981; Colbeck & Evans 1973), in the case of non-slip at the bed. Both accumulation distributions specified Q^* as a function of surface elevation H:

$$Q^* = Q_\infty - (Q_\infty - Q_0)\exp(-H/H^*), \tag{6.1}$$

where $Q^* \to Q_\infty > 0$ as $H \to \infty$, $Q^* = Q_0 < 0$ at $H = 0$ (not necessarily Q_M^*, which is the value at $\Delta = 0$) and H^* is a decay height. The equilibrium, or snow, line where $Q^* = 0$ is given by

$$H_e = H^* \ln(1 - Q_0/Q_\infty). \tag{6.2}$$

The two cases were

$$Q_L^*: \quad Q_0 = -6, \quad Q_\infty = 0.5, \tag{6.3a}$$

$$Q_S^*: \quad Q_0 = -3, \quad Q_\infty = 1, \tag{6.3b}$$

representing large margin ablation, small central accumulation, and small margin ablation, large central accumulation, respectively. For both Q_L^* and Q_S^*,

$$H^* = 0.25 \ (500\,\mathrm{m}): \quad H_e = 0.64 \ (1280\,\mathrm{m}) \quad \text{or} \quad 0.345 \ (690\,\mathrm{m}), \tag{6.4}$$

respectively. The first temperature distribution is

$$\bar{T}_1 = -0.8H + 0.5(H - Z)^2/\Delta = -0.8(\Delta + F) + 0.5\Delta y^2, \tag{6.5}$$

which has the surface properties

$$Z = H: \quad \bar{T}_1 = -0.8H, \quad \frac{\partial \bar{T}_1}{\partial H} = -0.8 \ (0.8\,\mathrm{K \ per \ 100\,m}), \quad \frac{\partial \bar{T}_1}{\partial Z} = 0, \tag{6.6}$$

with no heat flux through the surface, and basal properties

$$Z = F: \quad \bar{T}_1 = -0.3\Delta - 0.8F, \quad \frac{\partial \bar{T}_1}{\partial Z} = -1 \ (1\,\mathrm{K \ per \ 100\,m}), \tag{6.7}$$

representing a uniform heat flux into the base. Note, though, that $\partial^2 \bar{T}/\partial Z^2 = 1/\Delta$

is unbounded at the margin, so $\bar{s}$ is unbounded. Bounded $\bar{s}$ is given by the second distribution

$$\begin{aligned}\bar{T}_2 &= -0.8H + 0.5\{H - Z - 0.25[\Delta^2(H-Z) - \tfrac{1}{2}\Delta(H-Z)^2]\} \\ &= -0.8(\Delta + F) + 0.5\Delta\{y - 0.125\Delta^2 y(2-y)\},\end{aligned} \tag{6.8}$$

which has the surface properties

$$Z = H: \quad \bar{T}_2 = -0.8H, \quad \frac{\partial \bar{T}_2}{\partial H} = -0.8, \quad \frac{\partial \bar{T}_2}{\partial Z} = -0.5(1 - 0.25\Delta^2), \tag{6.9}$$

representing heat flux out of the surface for $\Delta < 2$ (4000 m) and heat flux in for $\Delta > 2$. On the bed,

$$Z = F: \quad \bar{T}_2 = -0.8F - 0.3\Delta - 0.0625\Delta^2, \quad \frac{\partial \bar{T}_2}{\partial Z} = -0.5 \text{ (0.5 K per 100 m)}, \tag{6.10}$$

again uniform heat flux into the base. The bed forms considered were

$$F = F_0 \exp(-cR^2), \tag{6.11}$$

with $c = 10$, a span of $2000c^{-1/2}\varepsilon^{-1} \sim 380$ km , and amplitude

$$\left.\begin{aligned}&\text{flat}: \quad F_0 = 0, \\ &\text{hump}: \quad F_0 = 0.1 \text{ (200 m)}, \\ &\text{basin}: \quad F_0 = -0.1.\end{aligned}\right\} \tag{6.12}$$

The main features of the solutions which serve to illustrate the distinctions are the margin radius (span) R_{M}, with unit $2000\varepsilon^{-1} \sim 1200$ km, and divide thickness $\Delta_{\mathrm{D}} = \Delta(0)$, with unit 2000 m. These parameters are given in tables 1 and 2 for the accumulation distributions Q^*_{L} and Q^*_{S}, respectively, which yield the most dramatic distinctions between the different solutions. The change of viscous law CE to SM produces moderate decreases of both the span R_{M} and divide thickness Δ_{D}, while the change of temperature distribution $\bar{T}_1$ to $\bar{T}_2$ produces moderate increases of both span R_{M} and thickness Δ_{D} for the accumulation distribution Q^*_{L}, but increase of the span R_{M} and decrease of the thickness Δ_{D} for the accumulation distribution Q^*_{S}. The span R_{M} and thickness Δ_{D} both increase slightly for the bed sequence hump–flat–basin. The change from accumulation Q^*_{L} to accumulation Q^*_{S} produces significant decreases in both span R_{M} and thickness Δ_{D}. The latter is an expected reflection of the decrease in equilibrium line from $H_{\mathrm{e}} = 0.64$ to 0.345, but there is a more significant decrease in the span R_{M} needed to achieve the net zero flux. An additional comparison has been made with three isothermal solutions for the SM viscous law with accumulation Q^*_{L} and a flat bed, shown in table 3 for the constant temperatures

$$\bar{T}_{\mathrm{A}} = -0.25 \text{ (}-5\text{ K)}, \quad \bar{T}_{\mathrm{B}} = -0.5 \text{ (}-10\text{ K)}, \quad \bar{T}_{\mathrm{C}} = -1 \text{ (}-20\text{ K)}, \tag{6.13}$$

giving three different constant rate factors $\bar{a}(\bar{T})$. Note that $\bar{T}_1$ ranges from 0 at the margin to -0.4 on the surface at the divide, while $\bar{T}_2$ ranges from 0 to -0.58. The constant temperature $\bar{T}_{\mathrm{A}} = -0.25$ produces a span R_{M} only a little less than those of $\bar{T}_1$ and $\bar{T}_2$, but a divide thickness much less, so the ice sheet profile, and consequent stress and velocity distribution, will be very different. The lower constant temperatures, more viscous ice, yield slightly larger thickness but smaller spans.

Comparisons between the non-slip and linear sliding law solutions have been made

Table 1. *Span R_M (unit 1200 km) and divide thickness Δ_D (unit 2 km) values for accumulation Q^*_L, non-slip*

	CE		SM	
	R_M	Δ_D	R_M	Δ_D
flat $\bar{T}_1$	0.52976	1.39131	0.45139	1.33355
flat $\bar{T}_2$	0.54038	1.43905	0.46433	1.38274
hump $\bar{T}_1$	0.50260	1.31954	0.40310	1.23217
hump $\bar{T}_2$	0.51574	1.36067	0.42015	1.27320
basin $\bar{T}_1$	0.54876	1.45783	0.48091	1.41016
basin $\bar{T}_2$	0.55790	1.51292	0.49172	1.46848

Table 2. *Span R_M (unit 1200 km) and divide thickness Δ_D (unit 2 km) values for accumulation Q^*_S, non-slip*

	CE		SM	
	R_M	Δ_D	R_M	Δ_D
flat $\bar{T}_1$	0.14319	0.62168	0.13184	0.60480
flat $\bar{T}_2$	0.14826	0.61782	0.13783	0.60154
hump $\bar{T}_1$	0.073426	0.41888	0.068716	0.40751
hump $\bar{T}_2$	0.075688	0.41617	0.071313	0.40521
basin $\bar{T}_1$	0.21709	0.79359	0.20245	0.78054
basin $\bar{T}_2$	0.22364	0.78908	0.21061	0.77620

Table 3. *R_M (unit 1200 km) and divide thickness Δ_D (unit 2 km) values for temperatures $\bar{T}_1$, $\bar{T}_2$, $\bar{T}_A$, $\bar{T}_B$, $\bar{T}_C$, non-slip*

	$\bar{T}_1$	$\bar{T}_2$	$\bar{T}_A$	$\bar{T}_B$	$\bar{T}_C$
R_M	0.45139	0.46433	0.44367	0.31784	0.20161
Δ_D	1.33355	1.38274	1.07693	1.12080	1.19929

for the temperature distribution $\bar{T}_2$ (yielding bounded $\bar{s}$) and constant temperatures $\bar{T}_A$, $\bar{T}_B$, $\bar{T}_C$, with the SM viscous law, and different combinations of accumulation Q^* of the form (6.1) and bed F of the form (6.11), with a constant friction coefficient $\bar{\Omega}$. First, consider a flat bed and a hump bed with amplitude 400 m:

$$F = 0 \quad \text{and} \quad F = 0.2\exp(-20R^2), \tag{6.14}$$

and accumulation with very small margin ablation

$$Q^*_V = 0.5 - 1.5\exp(-4H), \quad Q_0 = -1, \quad Q_\infty = 0.5, \quad H_e = 0.275\ (549\ \text{m}), \tag{6.15}$$

Table 4. *Span R_M (unit 1200 km) and divide thickness Δ_D (unit 2 km)values for non-slip and sliding, temperature $\bar{T}_2$*

$\bar{\Omega}$		∞ (non-slip)	100	25
flat	R_M	0.13852	0.22283	0.37299
	Δ_D	0.45253	0.52942	0.57295
hump	R_M	0.01452	0.09332	0.30368
	Δ_D	0.11158	0.18445	0.37390

Table 5. *Span R_M (unit 1200 km) and divide thickness Δ_D (unit 2 km) values for temperatures $\bar{T}_A$, $\bar{T}_B$, $\bar{T}_C$*

$\bar{\Omega}$		∞ (non-slip)	100	25
$\bar{T}_A = -0.25$	R_M	0.09680	0.20189	0.36137
	Δ_D	0.41849	0.52682	0.57255
$\bar{T}_B = -0.5$	R_M	0.06474	0.18565	0.35177
	Δ_D	0.42720	0.55943	0.58930
$\bar{T}_C = -1$	R_M	0.03692	0.17569	0.34655
	Δ_D	0.44826	0.59049	0.60020

Table 6. *Span R_M (unit 1200 km) and divide thickness Δ_D (unit 2 km) values for temperature $\bar{T}_2$*

$\bar{\Omega}$		∞ (non-slip)	10	5
flat	R_M	0.46433	1.23537	1.69636
	Δ_D	1.38274	1.67150	1.69472
hump	R_M	0.19942	1.19187	1.47738
	Δ_D	0.80297	1.69104	1.51772

with friction coefficients $\bar{\Omega} \equiv 100$ and 25, giving respective margin slip velocities for a flat bed

$$\text{flat}: \quad U_M = [-Q^*(0)/\bar{\Omega}(0)]^{1/2} = 0.1 \quad \text{and} \quad 0.2 \tag{6.16}$$

(in units 600 m yr^{-1}). The values of the span R_M and divide thickness Δ_D for temperature $\bar{T}_2$ are shown in table 4. As expected, the span R_M increases as the friction $\bar{\Omega}$ decreases, but also the thickness increases, producing a much larger ice sheet volume, not simply a redistribution into a longer, thinner sheet. Table 5 shows corresponding values at the constant temperatures $\bar{T}_A$, $\bar{T}_B$, $\bar{T}_C$ for a flat bed, and now it is seen

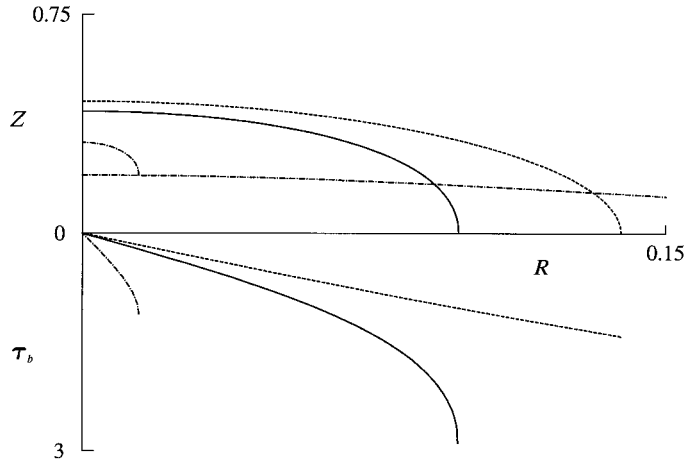

Figure 1. Profiles and basal tractions for non-slip temperature $T_A = -5$ K: ——, flat bed; and temperature T_2: – – –, flat bed; –·–·–, hump bed.

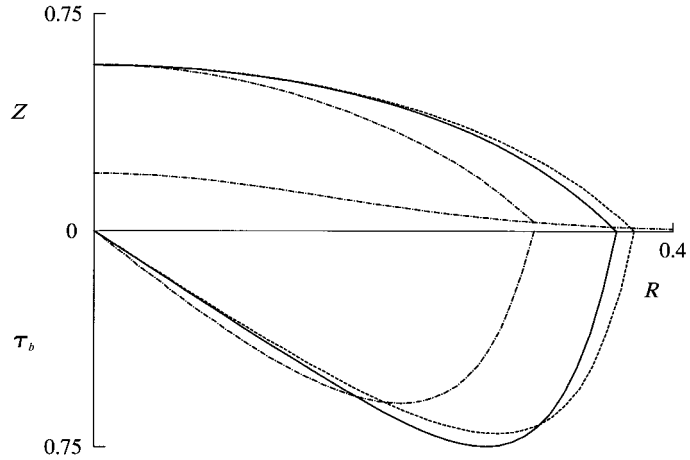

Figure 2. Profiles and basal tractions for sliding temperature $T_A = -5$ K: ——, flat bed; and temperature T_2: – – –, flat bed; –·–·–, hump bed.

that the isothermal results at $\bar{T}_A$ compares reasonably well with those for $\bar{T}_2$ shown in table 4 when sliding occurs, unlike the non-slip case.

Finally, consider a flat bed and a less sharp hump bed with amplitude 400 m:

$$F = 0 \quad \text{and} \quad F = 0.2\exp(-2R^2), \tag{6.17}$$

with accumulation Q_L^* defined by (6.3 *a*), and the much smaller friction coefficients $\bar{\Omega} \equiv 10$ and 5 giving margin slip velocities $U_M = 0.77$ (465 m yr^{-1}) and 1.1 (657 m yr^{-1}), respectively, for a flat bed.

Table 6 shows the span R_M and thickness Δ_D values for the temperature distribution $\bar{T}_2$. The low friction coefficient yield much larger spans, but not thickness, but the ratios to non-slip values are not dissimilar to those shown in table 4 for the higher friction coefficients; the main difference in the two tables is due to the change of accumulation Q^*. The ice sheet profiles and basal shear stress are now illustrated graphically for selected examples, namely for the temperature $\bar{T}_2$ (6.8) with accumulation Q_V^* (6.15) and the flat and hump beds (6.14), and $\bar{T}_A = -0.25$ (−5 K) with

accumulation Q^*_{V} for the flat bed. For the hump bed $Z = F$, both surface profile and bed form are drawn with the same line style and the surface terminates at a margin $Z = F > 0$. The three traction distributions are distinguished by the distinct spans R_{M} at which they end. The profiles and basal shear traction are shown in figure 1 for non-slip and in figure 2 for sliding with friction coefficient $\bar{\Omega} = 25$. The R and Z units are, respectively, 1200 km and 2 km, and the shear traction τ_{b} unit is $\varepsilon\rho g d_0 \sim 0.3$ Pa. Note the distinct R and τ_{b} scales in the two figures. The hump bed has the most dramatic effect in the non-slip solution since its amplitude 0.2 (400 m) is not much less than the equilibrium altitude $H_{\mathrm{e}} = 0.275$ (549 m) for the adopted accumulation Q^*_{V} (6.15).

Dr M. C. Thorne and Professor M. M. R. Williams of Electrowatt Engineering Services (UK) Ltd have shown considerable interest in the work, and I am grateful for their advice on the technical accuracy and presentation of this paper.

Nomenclature

a, a_0; $\bar{a}$	rate factor in viscous law
b, B	basal drainage flux
$B_{\mathrm{M}}(\,)$	thermal function
c_0, c_1	integrals
c	example parameter (B)
C	specific heat, 2×10^3 N m kg^{-1} K^{-1}
d_0	sheet thickness magnitude
D, D_0	strain-rate, unit 1 yr^{-1}
f, F	bed profile
g	constant gravity acceleration, 9.81 m s^{-2}
$g(\,)$	viscous function
G	geothermal heat flux, 4×10^{-2} W m^{-2}
h, H	surface profile
H^*, H_{e}	decay length and snow line elevation
I	integral
$\boldsymbol{j}$	unit horizontal vector
J	integral, shear stress invariant
$\boldsymbol{k}$	unit vertical vector
k	dimensionless parameter 0.0189
K_R, K_D	integrals
L	latent heat, 3.3×10^5 J kg^{-1}
$\boldsymbol{n}$, n	unit normal vector, normal coordinate
p, $\bar{p}$, $\bar{p}_{\mathrm{n}}$, $\bar{p}_{\mathrm{b}}$	pressure, dimensionless pressure and normal components, basal value
q, q_0; Q, $\bar{Q}$	surface accumulation flux; dimensionless forms
Q^*	net flux $Q - B$
Q_0, Q_∞	example Q^* values at $H = 0$, $H \to \infty$ (in Appendix B)
r, R; R_{M}	radial coordinate; margin radius
s, $\bar{s}$	heat and dimensionless heat source
$\boldsymbol{s}$	unit tangent vector
$S(\,)$	sliding function
t, $\bar{t}$; t	time and dimensionless time; normalized span variable
T, T_0; $\bar{T}$, $\tilde{T}$	temperature; dimensionless temperature
u_{n}	normal speed of surface
U, U_{b}	dimensionless radial velocity, basal value
$\boldsymbol{v}$, v_r, v_z	velocity and components
W	dimensionless vertical velocity
X	rectangular coordinate
y	normalized variable
z, Z	vertical coordinate

α	thermal parameter 0.491; example parameter (in Appendix B)
β	scaled bed slope F'
Γ	scaled surface slope H'
δ, $\delta_{\rm N}$, $\delta_{\rm s}$	asymptotic parameters
Δ, $\bar{\Delta}$	ice sheet thickness $H - F$
ω	stream function, example parameter (in Appendix B)
$\Omega(\,)$, $\bar{\Omega}(\,)$	sliding function
η	dimensionless variable
$\boldsymbol{\sigma}$, $\hat{\boldsymbol{\sigma}}$; $\bar{\boldsymbol{\sigma}}$	stress, deviatioric stress; dimensionless forms
σ_0	stress unit, 10^5 N m^{-2}
σ_{rr}, σ_{rz}, $\sigma_{\theta\theta}$, σ_{zz}	stress components
λ	thermal conductivity, 2.2 N K^{-1} s^{-1}
ρ	density, 917 kg m^{-3}
τ, $\tau_{\rm b}$	dimensionless shear stress magnitude, basal value
θ	polar angle
ϑ	dimensionless parameter 0.09
ε	dimensionless scaling parameter 0.001 66
ζ	$-\operatorname{sgn}\Gamma$
	subscripts M and D denote margin and divide values

Appendix A. Thickness profile equations and properties

For both non-slip and the linear sliding law (4.12) in steady flow, the profile equation (4.13) becomes an ordinary differential equation for the thickness $\Delta(R)$. With the derivative expressions (4.25) and (4.26), and definitions (4.21)–(4.24), this is

$$\begin{aligned}\frac{\mathrm{d}}{\mathrm{d}R}(\zeta I\Delta^2 + U_{\rm b}\Delta) + \frac{\zeta I\Delta^2 + U_{\rm b}\Delta}{R} = &-\left\{J\Delta^3 + \frac{\Delta}{\bar{\Omega}}\right\}(\Delta'' + \beta') + \zeta\Delta\Delta'(2I + K_{\rm D}\Delta)\\ &-\Delta'(\Delta' + \beta)\left\{J\Delta^2 + \frac{1}{\bar{\Omega}} - \frac{\Delta\bar{\Omega}'}{\bar{\Omega}^2}\right\} + \zeta K_R\Delta^2\\ &+\frac{1}{R}\left\{\zeta I\Delta^2 - \frac{\Delta(\Delta' + \beta)}{\bar{\Omega}}\right\} = Q^*, \qquad \text{(A 1)}\end{aligned}$$

where the non-slip equation is obtained by ignoring the $\bar{\Omega}$ terms, setting $\bar{\Omega}^{-1} = 0$.

As $R \to 0$ at the divide, $\Delta \to \Delta_{\rm D}$ (unknown), $Q^* \to Q^*_{\rm D}$ and

$$\beta,\ \Delta',\ \tau_{\rm b},\ U_{\rm b},\ g(\tau_{\rm b}y) \sim R, \qquad \text{(A 2)}$$

and since $g(0) = 0$, $g'(0) > 0$, $\bar{\Omega}(\Delta_{\rm D}) > 0$,

$$I,\ K_R,\ K_{\rm D} \sim R,\ J > 0. \qquad \text{(A 3)}$$

Thus, $R^{-1}\{\zeta I\Delta^2 - \Delta(\Delta' + \beta)/\bar{\Omega}\}$ remains bounded, $\to k_{\rm D}$ say, so that $(\zeta I\Delta^2 + U_{\rm b}\Delta) \sim k_{\rm D}R$ and $(\zeta I\Delta^2 + U_{\rm b}\Delta)' \sim k_{\rm D}$, then by (A 1), $2k_{\rm D} = Q^*_{\rm D}$, but $Q^*_{\rm D}$ depends on the unknown $\Delta_{\rm D}$ in general. However, in the shooting algorithm from the margin, each incorrect starting value $R_{\rm M}$ leads to non-vanishing Δ' at $R = 0$, and hence to an unbounded term in R^{-1}. The integration range during shooting is therefore ended a small distance (a free parameter) short of the divide, but the complete range is used for solution of (A 1) once the correct $R_{\rm M}$ is determined and $\Delta_{\rm D}$, and hence $Q^*_{\rm D}$ and $k_{\rm D}$, are constructed with the solution.

For the non-slip case, the transformations (5.7)–(5.10) are introduced to define a thickness function $\Delta = \tilde{\Delta}(t)$, which has bounded derivatives, asymptotic behaviour (5.11) as $R \to R_{\rm M}$, $t \to 0$, with coefficient $\delta_{\rm N}$ determined by (5.12) and (5.13),

and satisfies the differential equations (5.14) with κ derivative $G_{\rm N}(t,\tilde{\Delta},\kappa,R_{\rm M})$. From (A 1), ignoring the terms in $\bar{\Omega}$ and expressing $\Delta'(R)$, $\Delta''(R)$ in terms of $\kappa(t)=\tilde{\Delta}'(t)$ and $\kappa'(t)$, and assuming $\zeta=1$ over the entire range (a monotonic profile),

$$JG_{\rm N}=J[2R_{\rm M}\beta\eta\tilde{\Delta}-4R_{\rm M}^2t^2\beta']+\eta[4R_{\rm M}^2tK_R-2R_{\rm M}\tilde{\Delta}'K_{\rm D}+4R_{\rm M}^2tI/R] \\ +t^{-1}[J\{\tilde{\Delta}'(1-\eta\tilde{\Delta}'\}-4R_{\rm M}\eta(\eta\tilde{\Delta}'I+R_{\rm M}\eta^2Q^*)], \quad (A\,4)$$

where

$$\eta=t/\tilde{\Delta}. \quad (A\,5)$$

It was shown above that the term I/R is bounded as $R=R_{\rm M}(1-t^2)\to 0$, $t\to 1$, and given in terms of $\Delta_{\rm D}$ and $Q^*_{\rm D}$. The margin behaviour (5.11), (5.12), (5.17) must now be verified, confirming that the indeterminate t^{-1} term in (A 4) is bounded at $t\to 0$ with the limit of $G_{\rm N}$ given by (5.17).

At the margin $R=R_{\rm M}$, $t=0$, the variables Q^*, $\bar{T}$, $\bar{a}$, $\tau_{\rm b}$ and β have finite values $Q^*_{\rm M}$, $\bar{T}_{\rm M}$, $\bar{a}_{\rm M}$, $\tau_{\rm M}$, $\beta_{\rm M}$, and it is assumed that Q^*, $\bar{T}$ and $\bar{a}$ have bounded derivatives of their arguments. Near the margin then, as $t\to 0$ at fixed y, recalling the definition (4.19 *a*) of $\tilde{T}$,

$$\bar{T}=\bar{T}_{\rm M}+\frac{\partial\tilde{T}}{\partial\Delta}\kappa_{\rm M}t-\frac{\partial\tilde{T}}{\partial R}R_{\rm M}t^2+O(t^2), \quad (A\,6)$$

and hence

$$\bar{a}\sim\bar{a}_{\rm M}+\bar{a}'_{\rm M}B_{\rm M}t, \quad (A\,7)$$

where $B_{\rm M}(y)$ is defined by (5.10) and depends also on $R_{\rm M}$ and $\kappa_{\rm M}$. By (3.29), (5.8), (5.11) and (5.9), with $\zeta=1$ at M,

$$\tau_{\rm b}y=y\tilde{\Delta}\left\{\frac{\tilde{\Delta}'}{2R_{\rm M}t}-\beta\right\}\sim y\kappa_{\rm M}t(1+\delta_{\rm N}t\cdots)\left[\frac{\kappa_{\rm M}}{2R_{\rm M}t}(1+2\delta_{\rm N}t\cdots)-\beta_{\rm M}\right] \\ \sim\kappa_{\rm M}y\left[\frac{\kappa_{\rm M}}{2R_{\rm M}}+\left(\frac{3\kappa_{\rm M}\delta_{\rm N}}{2R_{\rm M}}-\beta_{\rm M}\right)t\right]\sim\tau_{\rm M}y+(3\tau_{\rm M}\delta_{\rm N}-\kappa_{\rm M}\beta_{\rm M})yt, \quad (A\,8)$$

and hence

$$g(\tau_{\rm b}y)\sim g(\tau_{\rm M}y)+g'(\tau_{\rm M}y)[3\tau_{\rm M}\delta_{\rm N}-\kappa_{\rm M}\beta_{\rm M}]yt. \quad (A\,9)$$

Incorporating the expansions (A 7) and (A 8) in the integral (4.21) for I, and noting the definitions (5.13) of c_1 and c_0, and the identity (5.6), shows that

$$I\sim-\frac{Q^*_{\rm M}}{2\tau_{\rm M}}+\{c_0+c_1[3\tau_{\rm M}\delta_{\rm N}-\kappa_{\rm M}\beta_{\rm M}]\}\bar{a}_{\rm M}t. \quad (A\,10)$$

In turn, from (4.18),

$$g_2[\,]=\Delta^2I\sim-Q^*_{\rm M}R_{\rm M}t^2\{-2Q^*_{\rm M}R_{\rm M}\delta_{\rm N}+\bar{a}_{\rm M}\kappa_{\rm M}^2t^3(c_0+c_1[3\tau_{\rm M}\delta_{\rm N}-\kappa_{\rm M}\beta_{\rm M}])\}t^3. \quad (A\,11)$$

Now, from (4.19 *b*), akin to (A 6),

$$Q^*\sim Q^*_{\rm M}+\left.\frac{\partial\tilde{Q}}{\partial\Delta}\right|_{\rm M}\kappa_{\rm M}t \quad (A\,12)$$

and so

$$\frac{1}{2}\int_R^{R_{\rm M}}R'Q^*\,{\rm d}R'\sim 2R_{\rm M}\int_0^t t'\left\{Q^*_{\rm M}+\left.\frac{\partial\tilde{Q}}{\partial\Delta}\right|_{\rm M}\kappa_{\rm M}t'\right\}{\rm d}t'\sim R_{\rm M}t^2\left\{Q^*_{\rm M}+\tfrac{2}{3}\kappa_{\rm M}\left.\frac{\partial\tilde{Q}}{\partial\Delta}\right|_{\rm M}t\right\}. \quad (A\,13)$$

Substituting these expansions in the integral property (5.2) with $U_b = 0$ verifies the balance at order t^2, and the balance at order t^3 confirms the expression (5.12) for δ_N. Since the expression (A 4) contains indeterminate terms as $t \to 0$, the limit (5.17) for G_N is used in some small interval from $t = 0$. Note that the differential equation (5.1) is the R derivative of the integral property (5.2), corresponding to $t^{-1}\,\mathrm{d}/\mathrm{d}t$, and hence the balance to order t^3 above as $t \to 0$ ensures the differential equation balance to order t, which determines δ_N in the expansion (5.11), and shows that the indeterminate terms in t^{-1} are bounded.

For the linear sliding law (4.12), or any sliding law with the friction proportional to pressure as pressure approaches zero, the margin slope is bounded and a linear transformation (5.30) is introduced simply to normalize the range. The new thickness function $\tilde{\Delta}(t)$ and its derivatives are defined by (5.30)–(5.33), with asymptotic expansions (5.34) and (5.35) as $t \to 0$. The differential equation (A 1) now includes terms involving the friction function $\bar{\Omega}(\Delta)$, which is strictly positive. $\Delta'(R)$ and $\Delta''(R)$ are now simply proportional to $\kappa(\tau)$ and $\kappa'(t) = G_s(t, \tilde{\Delta}, \kappa, R_M)$, respectively, by the linear relations (5.31), so (A 1) becomes, with the assumption $\zeta = 1$ over the entire range,

$$\begin{aligned}(J\tilde{\Delta}^2 + \bar{\Omega}^{-1})G_s = {} & -J\tilde{\Delta}(R_M^2\tilde{\Delta}\beta' - R_M\beta\kappa + \kappa^2) - R_M(2\kappa I + \tilde{\Delta}\kappa K_D - R_M\tilde{\Delta}K_R) \\ & + \kappa\tilde{\Delta}^{-1}\bar{\Omega}^{-2}(\bar{\Omega} - \tilde{\Delta}\bar{\Omega}')(R_M\beta - \kappa) - R_M^2\beta'\bar{\Omega}^{-1} - R_M^2\tilde{\Delta}^{-1}Q^* \\ & + R_M\bar{\Omega}^{-1}R^{-1}(R_M\tilde{\Delta}\bar{\Omega}I + \kappa - R_M\beta). \end{aligned} \tag{A 14}$$

It has been shown that the R^{-1} term is bounded as $R \to 0$, with limit depending on Δ_D and Q_D^*. For the margin behaviour, as $t \to 0$,

$$\tilde{\Delta} \sim \kappa_M t, \quad Q^* \sim Q_M^* + \left\{ \left.\frac{\partial \tilde{Q}}{\partial \Delta}\right|_M - \frac{R_M}{\kappa_M}\left.\frac{\partial \tilde{Q}}{\partial R}\right|_M \right\}\tilde{\Delta}, \tag{A 15}$$

$$\tau_b \sim \tilde{\Delta}, \quad g(\tau_b y) \sim \tilde{\Delta}, \quad I,\, \kappa_R,\, \kappa_D \sim \tilde{\Delta}, \quad J > 0, \tag{A 16}$$

$$\kappa \sim \kappa_M\left(1 + 2\frac{\delta_s}{\kappa_M}\tilde{\Delta}\right), \quad \beta \sim \beta_M - \beta_M'\frac{R_M}{\kappa_M}\tilde{\Delta}, \quad G_s \sim 2\kappa_M\delta_s, \tag{A 17}$$

and the balance of terms of order $\tilde{\Delta}^{-1}$ and unity in (A 14) becomes

$$\begin{aligned} 2\kappa_M\delta_s \sim {} & \tilde{\Delta}^{-1}\{\kappa_M[R_M\beta_M - \kappa_M] - R_M^2\bar{\Omega}(0)Q_M^*\} - 2R_M^2\beta_M' + \kappa_M - R_M\beta_M \\ & - 2\delta_s(2\kappa_M - R_M\beta_M) + \frac{\bar{\Omega}'(0)\kappa_M}{\bar{\Omega}(0)}(\kappa_M - R_M\beta_M) \\ & - R_M^2\left[Q_M^*\bar{\Omega}'(0) + \bar{\Omega}(0)\left\{\left.\frac{\partial \tilde{Q}}{\partial \Delta}\right|_M - \frac{R_M}{\kappa_M}\left.\frac{\partial \tilde{Q}}{\partial R}\right|_M\right\}\right]. \end{aligned} \tag{A 18}$$

Now by (5.32), which defines κ_M,

$$R_M^2 Q_M^*\bar{\Omega}(0) = \kappa_M(R_M\beta_M - \kappa_M), \tag{A 19}$$

and so the factor of $\tilde{\Delta}^{-1}$ in (A 17) vanishes and Q_M^* can be eliminated in favour of $\bar{\Omega}(0)$ when the order unity balance determines δ_s in the form (5.36).

Appendix B. Numerical algorithms and verification

Both non-slip and linear slip problems have been reduced to three first-order differential equations (5.14) and (5.33) for a thickness function $\tilde{\Delta}(t)$ on a normalized

range $0 \leqslant t \leqslant 1$, with bounded derivatives, of the form

$$\frac{\mathrm{d}\tilde{\Delta}}{\mathrm{d}t} = \kappa, \quad \frac{\mathrm{d}\kappa}{\mathrm{d}t} = G(\tilde{\Delta}, \kappa, t, R_{\mathrm{M}}), \quad \frac{\mathrm{d}R_{\mathrm{M}}}{\mathrm{d}t} = 0. \tag{B 1}$$

The $R-t$ transformations are, respectively, (5.7) and (5.30), and the functions G are G_{N} and G_{s} given by (A 4) and (A 14), with bounded R^{-1} terms as $R \to 0$ ($t \to 1$) at the divide which depend on the unknown divide thickness $\tilde{\Delta}_{\mathrm{D}}$ and net accumulation Q^*_{D}. The two-point boundary conditions are (5.15) for both

$$\begin{aligned} t = 0: &\quad \tilde{\Delta} = 0, \quad \kappa = \kappa_{\mathrm{M}}(R_{\mathrm{M}}) \quad \text{and} \\ t = 1: &\quad \kappa = 0, \end{aligned} \tag{B 2}$$

where R_{M} is the unknown margin radius and the transformed margin slopes are given, respectively, by (5.9) and (5.32), with (5.9) depending also on the margin tangential stress τ_{M} for non-slip given by the solution of (5.6). The margin limit of G is $2\kappa_{\mathrm{M}}\delta$, where δ_{N} and δ_{s} are given by (5.12) and (5.36). The integral property (5.2) of the solution becomes

$$\text{non-slip}: \quad I\Delta^2 = -\frac{1}{R}\int_R^{R_{\mathrm{M}}} R'Q^* \,\mathrm{d}R' = \frac{2R_{\mathrm{M}}}{R_{\mathrm{M}}(1-t^2)}\int_t^1 t'[1-(t')^2]Q^* \,\mathrm{d}t', \tag{B 3}$$

$$\text{linear slip} \begin{cases} I\Delta^2 - \dfrac{\Delta(\Delta'+\beta)}{\bar{\Omega}(\Delta)} = -\dfrac{1}{R}\displaystyle\int_R^{R_{\mathrm{M}}} R'Q^* \,\mathrm{d}R', \\ I\tilde{\Delta}^2 + \dfrac{\tilde{\Delta}(\tilde{\Delta}' - R_{\mathrm{M}}\beta)}{R_{\mathrm{M}}\bar{\Omega}(\tilde{\Delta})} = \dfrac{R_{\mathrm{M}}}{1-t}\displaystyle\int_t^1 (1-t')Q^* \,\mathrm{d}t'. \end{cases} \tag{B 4}$$

Note that I, Δ', $\beta \sim R$ as $R \to 0$, and the integrals in (B 3) and (B 4) $\sim R^2$ as $R \to 0$, so in addition to $\kappa = 0$ at $t = 1$, either $I\tilde{\Delta}^2$ or $I\tilde{\Delta}^2 + U_{\mathrm{b}}\tilde{\Delta}$ is also zero at $t = 1$.

The system (B 1) with two-point boundary conditions is solved numerically by a shooting algorithm from Numerical Recipes (Press *et al.* 1992), starting at $t = 0$ with a trial R_{M} which determines the initial slope κ_{M}, testing the predicted magnitude of a positive combination of κ and I or $I + U_{\mathrm{b}}/\tilde{\Delta}$ at $t = 1 - \varepsilon_r$, and iterating until the combination is sufficiently small. The offset ε_r avoids the unbounded terms in G obtained at $t = 1$ when R_{M} is not the correct margin location, and it is also necessary to restrict the magnitude of G, so that the terms do not become too large and prevent a useful iteration. Once an accurate R_{M} is determined, the system is solved as an initial value problem from $t = 0$ to $t = 1$, using the known asymptotic behaviour of the bounded terms in R^{-1} as $t \to 1$, which verifies that κ and I vanish at $t = 1$. Various non-physical G allowing exact solutions were first used to test and refine the algorithm.

A major, and complex, part of the problem is the construction of G at each step of the iteration, including the asymptotic coefficient δ and the margin traction τ_{M} in the case of non-slip. The non-slip and slip problems have distinct constructions and require separate test problems. These can be generated from the integral property (B 3) or (B 4). If Q^* is prescribed as an explicit function of R only, then the common integral in (B 3) and (B 4) can be evaluated and the limit R_{M} necessary for it to vanish (zero net ice flux into the steady profile) determined. Recalling that I defined by (4.21) involves $g(\tau_{\mathrm{B}}y)$, and τ_{b} is linear in Γ, and hence linear in $\Delta'(R)$, both (B 3) and (B 4) become first-order differential equations for $\Delta(R)$. The choice

of a linear viscous function $g(\tau)$, constant factor $\bar{a}$, particular bed forms $F(R)$ and friction function $\bar{\Omega}(\Delta)$ allow exact solutions.

Consider

$$Q^* = Q_0(1 - R/R_s) = 0 \quad \text{at } R = R_s, \tag{B 5}$$

then

$$-\frac{1}{R}\int_R^{R_M} R'Q^*\,\mathrm{d}R' = \frac{1}{R}\int_0^R R'Q^*\,\mathrm{d}R' = \tfrac{1}{2}Q_0R\left(1 - \frac{2R}{3R_s}\right), \tag{B 6}$$

which vanishes at

$$R = R_M = \tfrac{3}{2}R_s, \tag{B 7}$$

so the divide and margin accumulations are

$$Q_D^* = Q_0, \quad Q_M^* = -\tfrac{1}{2}Q_0. \tag{B 8}$$

With a constant rate factor, linear viscous function and bed elevation proportional to thickness,

$$\bar{a} = 1, \quad g(\tau) = g_0\tau, \quad F = \alpha\Delta, \tag{B 9}$$

by (4.12), (4.18) and (4.21),

$$g_2[\,] = \Delta^2 I = -\tfrac{1}{3}g_0\Delta^3(1+\alpha)\Delta'(R). \tag{B 10}$$

The non-slip equation (B 3) for $\alpha = 0$ becomes

$$[\Delta^4(R)]' = -\frac{6Q_0R}{g_0}\left(1 - \frac{R}{R_M}\right), \tag{B 11}$$

with solution vanishing at $R = R_M$,

$$\Delta^4(R) = \frac{Q_0}{g_0R_M}(R_M - R)(R_M^2 + RR_M - 2R^2), \tag{B 12}$$

and applying the transformation (5.7),

$$\tilde{\Delta}^4(t) = \frac{Q_0R_M^2t^4}{g_0}(3 - 2t^2). \tag{B 13}$$

Thus

$$\tilde{\Delta}(t) = \kappa_M t(1 - \tfrac{2}{3}t^2)^{1/4}, \tag{B 14}$$

where

$$\kappa_M = \left\{\frac{3Q_0R_M^2}{g_0}\right\}^{1/4}, \quad \delta_N = 0 \tag{B 15}$$

and, by (5.9),

$$\tau_M = \left\{\frac{3Q_0}{4g_0}\right\}^{1/2}, \tag{B 16}$$

which satisfies (5.6) with the margin accumulation given by (B 8). Since β is a bounded bed slope, a bed elevation proportional to thickness ($\alpha \neq 0$) is not valid for non-slip which has unbounded $\Delta'(R)$ at the margin.

For the linear slip equation (B 4), consider a friction coefficient

$$\bar{\Omega}(\Delta) = \Omega_0\exp(\omega\Delta^2), \tag{B 17}$$

then with the relations (B 5)–(B 10) again, (B 4) becomes

$$[\exp(-\omega\Delta^2) + \tfrac{1}{3}g_0\Omega_0\Delta^2]2\Delta\Delta' = -\frac{Q_0\Omega_0 R}{1+\alpha}\left(1 - \frac{R}{R_{\rm M}}\right), \tag{B 18}$$

which, with $\Delta(R_{\rm M}) = 0$, has solution

$$f(\Delta) = 1 - \exp(-\omega\Delta^2) + \tfrac{1}{6}g_0\omega\Omega_0\Delta^2 = \frac{Q_0\omega\Omega_0}{6R_{\rm M}(1+\alpha)}(R_{\rm M} - R)^2(2R + R_{\rm M})$$

$$= \frac{Q_0\omega\Omega_0 R_{\rm M}^2}{6(1+\alpha)}t^2(3 - 2t). \tag{B 19}$$

Now, for $0 < t \leqslant 1$,

$$0 < \frac{Q_0\omega\Omega_0 R_{\rm M}^2}{6(1+\alpha)}t^2(3 - 2t) < \frac{Q_0\omega\Omega_0 R_{\rm M}^2}{6(1+\alpha)}, \tag{B 20}$$

while $f(0) = 0$ and $f'(\Delta) > 0$, and $f'(\Delta) \to \infty$ as $\Delta \to \infty$, so (B 19) has a unique positive root Δ for each t in $0 < t \leqslant 1$, which can be accurately calculated by a straightforward root finding algorithm. In turn, Δ' and $\beta = \alpha\Delta'$ are given by (B 18), then Δ'' and $\beta' = \alpha\Delta''$ by differentiation with respect to R, since β and β' are required in (A 14) for $G_{\rm s}$ in the direct solution algorithm. Using the asymptotic expansion (5.33) as $t \to 0$ for $\tilde{\Delta}(t)$ in $f(\Delta) = f(\tilde{\Delta})$, and comparing coefficients of t^2 and t^3 in (B 19), shows that

$$\kappa_{\rm M} = \left\{\frac{Q_0\Omega_0 R_{\rm M}^2}{2(1+\alpha)}\right\}^{1/2}, \quad \delta_{\rm s} = -\tfrac{1}{3}, \tag{B 21}$$

which confirms the margin slope expression (5.32).

Both the non-slip and the linear sliding law algorithms for solution of (B 1) determined accurately the solutions (B 12) and (B 19), respectively, for a variety of parameters. These test solutions are restricted to a linearly viscous law and to isothermal conditions, not therefore confirming the correct incorporation of $g'(\tau_{\rm b}y)$ and the many $\bar{T}$ derivatives in the construction. However, the respective integral properties (B 3) and (B 4) are verified at each integration step t in the direct solution, comparing the net accumulation integral with the viscous and sliding terms constructed from the calculated profile and derivatives, confirming that an accurate solution of the differential equations (B 1) has been determined.

A final numerical procedure is the calculation of the heat source $\bar{s}$ given by (4.1), which is necessary in the energy balance to yield the temperature distribution prescribed in the present analysis. The new feature is the calculation of the vertical velocity W given by (4.2), which, by (4.4) and (4.9) with $\zeta = 1$, becomes

$$W = -B - \left(\frac{\partial g_2}{\partial R} + \frac{g_2}{R}\right) - \frac{1}{R}\frac{\partial}{\partial R}[R(Z - F)U_{\rm b}], \tag{B 22}$$

where $g_2(R, Z)$ is defined by (4.14). In terms of the transformation (4.16), g_2 is expressed by

$$\tilde{g}_2(R, y) = \Delta^2\int_y^1 (y' - y)\bar{a}(\bar{T}')g(\tau_{\rm b}y')\,{\rm d}y', \tag{B 23}$$

and

$$\left.\frac{\partial g_2}{\partial R}\right|_Z = \left.\frac{\partial \tilde{g}_2}{\partial R}\right|_y + \frac{H' - y\Delta'}{\Delta}\left.\frac{\partial \tilde{g}_2}{\partial y}\right|_R. \tag{B 24}$$

By (4.7) and (4.8),

$$\left.\frac{1}{\Delta}\frac{\partial \tilde{g}_2}{\partial y}\right|_R = -\left.\frac{\partial g_2}{\partial Z}\right|_R = U_\mathrm{b} - U, \tag{B 25}$$

and from (B23),

$$\begin{aligned}\frac{\partial \tilde{g}_2}{\partial R} = {} & 2\Delta\Delta' \int_y^1 (y' - y)\bar{a}(\bar{T}')g(\tau_\mathrm{b} y')\,\mathrm{d}y' \\ & -\Delta^2[\Delta'(\Delta' + \beta) + \Delta(\Delta'' + \beta')] \int_y^1 (y' - y)\bar{a}(\bar{T}')g'(\tau_\mathrm{b} y')\,\mathrm{d}y' \\ & +\Delta^2 \int_y^1 (y' - y)\bar{a}'(\bar{T}')g(\tau_\mathrm{b} y')\left[\frac{\partial \tilde{T}}{\partial R} + \Delta'\frac{\partial \tilde{T}}{\partial \Delta}\right]\mathrm{d}y',\end{aligned} \tag{B 26}$$

recalling the prescription (4.19), $\bar{T} = \tilde{T}(R, \Delta, y, R_\mathrm{M})$. The remaining derivative is

$$\frac{1}{R}\frac{\partial}{\partial R}[R(Z - F)U_\mathrm{b}] = -\beta U_\mathrm{b} + \Delta(1 - y)\frac{\partial U_\mathrm{b}}{\partial R} + \frac{\Delta(1 - y)}{R}U_\mathrm{b}. \tag{B 27}$$

Since $\tilde{g}_2 \sim R$ and $U_\mathrm{b} \sim R$ as $R \to 0$, it follows that $\tilde{g}_2/R$ and $U_\mathrm{b}/R \sim \partial \tilde{g}_2/\partial R$ and $\mathrm{d}U_\mathrm{b}/\mathrm{d}R$, respectively, which can be used to replace the bounded indeterminate terms in R^{-1} as $R \to 0$. As $R \to R_\mathrm{M}$, bounded $\bar{s}$ requires bounded $\partial \bar{T}/\partial Z$ and $\partial^2 \tilde{T}/\partial Z^2$, and hence bounded $\Delta^{-1}\partial \tilde{T}/\partial t$ and $\Delta^{-2}\partial^2 \tilde{T}/\partial y^2$ as $\Delta \to 0$, which are restrictions on a sensible prescribed $\tilde{T}(R, \Delta, y, R_\mathrm{M})$.

References

Colbeck, S. C. & Evans, R. T. 1973 A flow law for temperate glacier ice. *J. Glaciol.* **12**, 71–86.

European Ice Sheet Modelling Initiative Workshop, Aussois 1994 *Proc. Mechanical Properties of Polar Ice and Ice Sheet Modelling* (convenors: C. Ritz & L. W. Morland) (ed. C. S. M. Doake, British Antarctic Survey, Cambridge).

Fowler, A. C. 1977 Glacier dynamics. D.Phil. thesis, Oxford University.

Fowler, A. C. 1979*a* A mathematical approach to the theory of glacier sliding. *J. Glaciology* **23**, 131–141.

Fowler, A. C. 1979*b* The use of a rational model in the mathematical analysis of a polythermal glacier. *J. Glaciology* **24**, 443–456.

Fowler, A. C. & Larson, D. A. 1978 On the flow of polythermal glaciers. I. Model and preliminary analysis. *Proc. R. Soc. Lond.* A **363**, 217–242.

Glen, J. W. 1955 The creep of polycrystalline ice. *Proc. R. Soc. Lond.* A **228**, 519–538.

Hindmarsh, R. C. A., Morland, L. W., Boulton, G. S. & Hutter, K. 1987 The unsteady plane flow of ice-sheets: a parabolic problem with two moving boundaries. *Geophy. Astrophys. Fluid Dyn.* **39**, 183–225.

Hutter, K. 1981 The effect of longitudinal strain on the shear stress of an ice sheet: in defence of using stretched co-ordinates. *J. Glaciol.* **27** 39–56.

Hutter, K. 1982*a* Dynamics of glaciers and large ice masses. *A. Rev. Fluid Mech.* **14**, 87–130.

Hutter, K. 1982*b* A mathematical model of polythermal glaciers and ice sheets. *Geophys. Astrophys. Fluid Dyn.* **21**, 201–224.

Hutter, K. 1983 *Theoretical glaciology.* Dordrecht: Reidel.

Hutter, K., Legerer, F. & Spring, U. 1981 First-order stresses and deformation in glaciers and ice sheets. *J. Glaciol.* **27**, 227–270.

Hutter, K., Yakowitz, S. & Szidarovsky, F. 1987 Coupled thermomechanical response of an axisymmetric ice sheet. *Water Res.* **23**, 1327–1339.

Huybrechts, P. A., Payne, A. J. & the EISMINT Intercomparison Group. 1996 The EISMINT benchmarks for testing ice-sheet models. *A. Glaciol.* **23**, 1–14.

Johnson, I. R. 1981 The steady profile of an axisymmetric ice sheet. *J. Glaciol.* **27**, 25–37.

Lliboutry, L. A. 1969 The dynamics of temperate glaciers from the detailed viewpoint. *J. Glaciol.* **8**, 185–205.

Mellor, M. & Testa, R. 1969 Effect of temperature on the creep of ice. *J. Glaciol.* **8**, 131–145.

Morland, L. W. 1984 Thermomechanical balances of ice sheet flows. *Geophys. Astrophys. Fluid Dyn.* **29**, 237–266.

Morland, L. W. 1987 Unconfined ice sheet flow. In *Proc. Workshop Dynamics of the West Antaractic Ice Sheet, Utrecht 1985* (ed. C. J. Van der Veen & J. Oerlemans), pp. 99–116. Dordrecht: Reidel.

Morland, L. W. 1993 The flow of ice sheets and ice shelves, CISM lectures 1992, no. 337. In *Continuum mechanics in environmental sciences and geophysics* (ed. K. Hutter), pp. 402–466. Berlin: Springer.

Morland, L. W. & Johnson, I. R. 1980 Steady motion of ice sheets. *J. Glaciol.* **25**, 229–246.

Morland, L. W. & Johnson, I. R. 1982 Effects of bed inclination and topography on steady isothermal ice sheets. *J. Glaciol.* **28**, 71–90.

Morland, L. W. & Shoemaker, E. M. 1982 Ice shelf balances. *Cold Reg. Sci. Tech.* **5**, 235–251.

Morland, L. W. & Smith, G. D. 1984 Influence of non-uniform temperature distribution on the steady motion of ice sheets. *J. Fluid Mech.* **140**, 113–133.

Morland, L. W. & Zainuddin, R. 1987 Plane and radial ice-shelf flow. In *Proc. Workshop Dynamics and the West Antarctic Ice Sheet, Utrecht 1985* (ed. C. J. Van der Veen & J. Oerlemans), pp. 117–140. Dordrecht: Reidel.

Press, W. H., Teukolsky, S. A., Vetterling, W. T. & Flannery, B. P. 1992 *Numerical recipes in fortran*, 2nd edn. Cambridge Univeristy Press.

Smith, G. D. & Morland, L. W. 1981 Viscous relations for the steady creep of polycrystalline ice. *Cold Reg. Sci. Tech.* **5**, 141–150.

Received 17 July 1996; accepted 13 December 1996